Drained triaxial testing of shales: insight from the Opalinus Clay

Pierre Delage, Malik Belmokhtar

Drained triaxial testing of shales: insight from the Opalinus Clay

Pierre Delage[1], Malik Belmokhtar[1,2]

[1] Ecole des Ponts ParisTech, Navier-CERMES, France
corresponding author: pierre.delage@enpc.fr - Orcid number 0000-0002-2101-5522

[2] now at BG Ingénieurs Conseils, Ivry sur Seine, France

Abstract

The investigation of the mechanical behaviour of swelling claystones and shales is challenging because of their very low permeability and of their high sensitivity to changes in water content. The former makes it difficult to carry out triaxial tests with controlled homogeneous water pore pressure fields, the latter results in some possible effects of swelling when unsaturated extracted specimens are re-saturated prior to being tested. This work presents some data from drained triaxial tests performed on specimens of Opalinus Clay, designated as host rock for radioactive waste disposal in Switzerland, extracted at shallow depth close to the city of Lausen. The data are compared to those recently published from undrained triaxial tests on specimens from the same place, and also to two sets of recent data independently obtained on Opalinus Clay specimens sourced from greater depth at the Mt Terri Underground Research Laboratory. By comparing the data of our drained tests on Lausen specimens to those from specific undrained tests in which swelling has been prevented, quite a good comparability in shear strength is observed at confining effective stresses larger than 5 – 6 MPa. This is related to the small magnitude of the swelling occurring above this stress during the specimen hydration in drained tests. The question of the possible linearity of the shear strength criterion at low stress is also discussed with respect to both our data and other published ones. It is suggested that undrained tests be also carried out at low confining stresses to investigate if some perturbations due to hydration swelling occur in this area, that could result in a non-linear shape of the criterion. The change in Young modulus and Poisson coefficient with stress are also discussed, and the data on Opalinus Clay are compared to those of the Callovo-Oxfordian claystone from France, evidencing interesting similarities in terms of shear strength properties and Young's moduli.

Keywords: shales, mechanical properties, triaxial testing, radioactive waste

1. Introduction

The investigation of the mechanical properties of low permeability claystones has been carried out in the field of conventional oil and gas production, in link with borehole stability issues (e.g. Steiger and Leung 1991; Schmitt et al. 1994; Aoki et al. 1995; Ewy et al. 2003, Sarout and Detournay 2011, Islam and Skalle 2013) and tunnelling issues (e.g. Einstein 2000; Bonini et al. 2009; Wild and Amann 2018b). Further attention has been more recently paid to claystones and shales with respect to the sequestration of CO_2 (Busch et al. 2008), the production of shale oil and gas (e.g. Ewy et al. 2003; Eseme et al. 2007; Villamor-Lora et al. 2016, Douma et al. 2020) and the deep geological disposal of radioactive waste on clays and claystones, a field in which many investigations have been recently carried out on two clay rocks designated as host rocks in Europe, the Opalinus Clay (Switzerland) and the Callovo-Oxfordian claystone (France). Triaxial testing of clay rocks and shales is challenging given their low permeability and their sensitivity to change in stress and water content during core extraction, specimen trimming and re-saturation prior to testing.

In this paper, a series of drained tests were carried out on Opalinus Clay specimens extracted at shallow depth close to the city of Lausen in Switzerland, and the data are compared to those of undrained tests carried out by Giger et al. (2018) on specimens from the same location. Further understanding of the mechanical properties of the Opalinus Clay is also gained by considering the data of Favero et al. (2018) and Wild and Amman (2018) on deep specimens from the Mt Terri area.

2. Triaxial testing of clay rocks

Clay rocks have sometimes been tested by adopting standard rock mechanics testing methods, with little consideration given to saturation and drainage issues, sometimes resulting in overestimating their mechanical parameters due to both incomplete saturation or poor drainage during shearing (e.g. Chiu et al. 1983, Menaceur et al. 2015). Another challenge is the difficulty of keeping homogeneous pore pressure fields within the specimens during the tests, in particular during drained triaxial tests. An alternative,

currently used in soil mechanics, is to run undrained tests with pore pressure measurements. Undrained tests are faster to run and give access to what are called “undrained parameters” through a coupled global hydromechanical response of the saturated specimen (solid + water). Some specimen material parameters can be derived from the monitored pore pressure changes, whereas some others (plastic volume changes, creep properties) are more difficult to obtain. Conversely, drained tests provide the mechanical response of the rock skeleton, allowing for a direct determination of these parameters.

In undrained tests, it is mandatory to correct the pore pressure data from the effects of the water volume contained in the porous disks and in the ducts connected to the specimen, as shown in some pioneering contributions from soil mechanics (Wissa 1969 and Bishop 1972) and in claystones (Chiu et al. 1983, Ghabezloo and Sulem 2010 and Sarout and Detournay 2011). These effects are minimised by putting the pressure gauge in direct contact with the specimen (Ewy 2015, 2018), as recently done by Giger et al. (2018) to investigate the mechanical properties of the Opalinus Clay with undrained triaxial tests run at a low axial strain rate of 2×10^{-7} s^{-1}. Undrained tests on the Opalinus Clay have also been carried out by Sarout et al. (2014) and Wild and Amman (2018a).

Drained and undrained shear tests require the saturation of specimens that may have been affected by some loss of moisture due to the combined effects of coring, storage, specimen preparation and mounting (Chiu et al. 1983, Monfared et al. 2011, Sarout et el. 2014, Ewy 2015, Wild et al. 2017). This stage is particularly critical for swelling shales like the Opalinus Clay or the Callovo-Oxfordian claystone from France, that are both sensitive to changes in water content (e.g. Chiarelli et al. 2003, Valès et al. 2004, Zhang and Rothfuchs 2004, Pham et al. 2007, Zhang et al. 2012) and prone to swelling when put in contact with water (Mohajerani et al. 2011, Wan et al. 2013, Ferrari et al. 2014, Menaceur et al. 2016, Wild et al. 2017). There are various options to minimize the effects of swelling. Monfared et al. (2011) proposed to set-up the specimen on dry porous disks prior to re-saturating it under stress conditions close to in-situ, which resulted in a

swelling of around 1 – 1.5% (see also Menaceur et al. 2015, Wild et al. 2017, Belmokhtar et al. 2018). Given that swelling has been observed to result in the developments of micro-cracks (Mohajerani et al. 2011, Bornert et al. 2010, Wang et al. 2013, Wan et al. 2013, Menaceur et al. 2016b, Delage and Tessier 2020), this saturation procedure may result in some damage, leading to a possible under-estimation of the mechanical properties. An alternative is the re-saturation at (almost) constant volume, as carried out by Favero et al. (2018) on a specimen of Opalinus Clay from the shaly facies of Mt Terri, who observed that applying an isotropic effective confining stress of 3.5 MPa allowed to reduce swelling to 0.4 – 0.5%. Another approach to avoid specimen swelling was developed by Ewy et al. (2018) and adopted in the undrained tests carried out by Giger et al. (2018) on Opalinus Clay specimens. In this approach, they previously equilibrated their specimens at high relative humidity (up to 98%) and high degree of saturation prior to put them in contact with a pore pressure gauge to run the undrained tests.

Low enough strain rates are necessary to perform drained triaxial test on low permeability specimens. As shown by Gibson and Henkel (1954), based on the solution of the one dimensional consolidation of fine-grained soils (Terzaghi & Fröhlich, 1936), the degree of pore pressure dissipation is controlled by the non-dimensional parameter $T = C_v\ t/h^2$ (in which C_v is the consolidation coefficient, t the time variable and h the drainage length). Gibson and Henkel (1954) analytically showed that 99% pore pressure dissipation was achieved when $T = 1.67$. Satisfactory drainage is hence controlled by both the specimen permeability (contained in C_v) and the boundary conditions (defined by the drainage length h). This approach has been used for clay rocks by Chiu et al. (1983), who found that a strain rate of 8×10^{-7} s^{-1} was appropriate to ensure satisfactory dissipation of excess pore pressure on a triaxial specimen of Melbourne mudstone ($C_v = 3 \times 10^{-6}$ m/s^2, specimen 28.5 mm in diameter and 57 mm in height) drained at bottom (h = 57 mm). In their investigation of the strain rate effects on the mechanical characteristics of Kimmeridge Bay shale (mean permeability of 8×10^{-21} m^2 under 10 MPa), Swan et al. (1989) performed some poroelastic

finite elements calculations of the excess pore pressure generated during triaxial testing. They showed that, with a specimen of 50 mm height and 25 mm diameter with lateral drainage (drainage length 12.5 mm), an axial strain rate of 8.3×10^{-7} s^{-1} was satisfactory. Wu et al (1997) investigated the properties of the Pierre II shale with specimens of the same size, and found that a rate of 3×10^{-8} s^{-1} was satisfactory to ensure homogeneous pore pressure during undrained tests. Islam and Skalle (2013) performed a series of triaxial tests with standard triaxial specimens (76 mm height and 38 m diameter) of Pierre I shale with strain rates of $1–2 \times 10^{-7}$ s^{-1} for undrained tests and 2×10^{-8} s^{-1} for drained tests. Belmokhtar et al. (2018) ran some tests on standard triaxial specimens of the Callovo-Oxfordian (COx) claystone (permeability 10^{-20} m^2) with a reduced drainage length of 19 mm, and showed, based on poroelastic calculations, that a rate of 6.6×10^{-8} s^{-1} was satisfactory.

Undrained tests can be faster, but their strain rates should be slow enough to allow for pore pressure homogeneity, particularly with respect to friction effects that may occur on both the top and the bottom of the specimen in contact with the porous disks. This aspect has been investigated among others by Blight (1963) and Nakase and Kamei (1986), who showed that too fast strain rates tended to provide over-estimated values of undrained strength, and that strain rates smaller than 10^{-6} s^{-1} were satisfactory in standard triaxial samples of clays (38 mm diameter and 76 in height). In their undrained tests on Opalinus Clay samples, Giger et al. (2018) also tested various strain rates, showing that 2×10^{-7} s^{-1} were satisfactory for the size of their samples (19 mm diameter and 38 mm height), whereas some over-estimation was observed at larger rates (2×10^{-5} s^{-1} and 2×10^{-6} s^{-1}).

In an attempt to reduce the variability in shear strength properties of the Opalinus Clay observed in previous investigations, drained tests have been carried out on specimens from various origins by various authors. More recently, Favero et al. (2018) tested specimens of 100 mm height and 50 mm diameter at a strain rate of 3×10^{-8} s^{-1} with bottom drainage (h = 25mm); Wild and Amann (2018a) tested specimens of 133 mm height and 67mm diameter with lateral drainage (h =

33.5 mm) at a strain rate of 10^{-8} s^{-1}; Giger et al. (2018) tested specimens of 38 mm in height and 19 mm in diameter, with side drains (h = 9.5 mm, C_v = 3.4 x 10^{-9} m/s^2) at a strain rate of 2 x 10^{-8} s^{-1}.

In this paper, a series of drained triaxial tests on specimens of the same origin as those tested by Giger et al. (2018) is carried out to complete the existing data base and to compare the drained data with the undrained ones of Giger et al. (2018). The specimens were extracted from the Lausen borehole, at a depth of around 33 m. Compared to the 250 – 300 m deep specimens from the Mt Terri Underground Research Laboratory (URL) that are more often investigated (e.g. Naumann et al. 2007, Corkum and Martin 2007, Bock 2009, Bossart 2011, Favero et al. 2018, Wild and Amman 2018), the Lausen borehole was drilled at shallower depth to investigate the possible unloading effects resulting from the long-term uplift of the Opalinus Clay layer. It was shown that unloading and weathering only affected the layer down to a depth of around 28 m, whereas specimens at slightly larger depth have not been significantly affected, with the same bulk wet density (2.47 Mg/m^3) as specimens from deeper boreholes (Crisci et al. 2019, Giger et al. 2018).

3. Materials and methods

3.1. The Opalinus Clay

The Opalinus Clay is a low permeability (k = 10^{-12} - 10^{-14} m/s) sedimentary clay rock deposited in a marine environment about 180 million years ago (Middle Jurassic, Lower Aalenian). The shaly facies of Opalinus clay at the Mont Terri Underground research laboratory is mainly composed of clay minerals (50-80%), quartz (10-20%), carbonates (5-20%), and feldspar (0-5%) (Thury and Bossart, 1999; Bossart, 2011; Klinkenberg et al., 2009). The clay fraction is made up of illite-smectite mixed layers (5 – 15%), illite (15 – 25%), chlorite (5 – 15%) and kaolinite (20 – 30%) (Nagra, 2002, Bossart, 2005, Mazurek et al. 2008, Klinkenberg et al., 2009). Due to compaction and long-term diagenesis, the Opalinus clay presents apparent bedding planes and exhibits transverse isotropic properties (Corkum and Martin 2007, Nadri et al. 2012, Sarout et al. 2014, Favero et al. 2018).

The specimens tested in this work come from cores 5 and 7 that were extracted close to the city of Lausen (Northern Switzerland) at shallow depths, between 30.4 and 31.4 m for core 5 and between 36.4 and 37.2 m for core 7. At this depth, the pore pressure is estimated at 0.3 MPa and the mean stress at 1.3 MPa, resulting in a 1 MPa mean effective stress (Giger, personal communication). Cores were extracted perpendicular to bedding using a water-based drilling fluid with a polymer additive. Core sections of 10 cm in diameter and 102 cm (core 5) and 80 cm (core 7) in length were wrapped and sealed in aluminium foil and resin-impregnated into a plastic barrel within approximately fifteen minutes after recovery, to preserve their water content.

3.2. Mineralogical, chemical and physical characterisation of the specimens

Figures 1 and 2 present some photos and X-Ray computed tomography (CT) scans that were performed prior to sending the cores to the lab, 11 days after extraction from the ground to check for integrity and internal variability of the cores. Imaging was performed with a Somatom Definition AS 64 and tube voltage was 140 kV. All scans were performed using the automatic dose modulation software (CARE Dose 4D), with collimation equal to 64→0.6 mm and a voxel size of 0.25 → 0.25 → 0.4 mm on the whole specimens. A virtual cross-section through the centre of the core was generated from the 3D CT images (Figure 1b and 2b). This cross-section allowed the detection of cracks with a crack spacing wider than voxel-size. These cracks were carefully avoided during the selection of the subsample that was subsequently investigated.

In Figure 1, the CT scans of core 5 show 4 discontinuities (Figure 1b) that became quite apparent after opening (Figure 1e). One can observe 3 additional discontinuities not detected by CT scanning, resulting in a core truncated into 8 sections. Note that core 5 was opened 4 months after core reception, with a water content w = 4.51% and a degree of saturation S_r = 86%, compared to w = 4.65% and S_r = 90.8% for core 7. Water contents were determined by putting some cuttings (1

179 or 2 centimetres long, around 5 mm thick) obtained from specimen trimming in the oven at 105°C
180 during 48 h, as commonly done in claystones (ISRM 1979, Wild and Amman 2018).

181 The photo of core 7 after reception and opening (Figure 2a) shows two discontinuities parallel
182 to bedding plane, whereas only the bottom one was detected in the CT scan (b, red arrow).

183 The grey-value of a given CT image voxel represents the mean material density related to the
184 volume fractions of different minerals and pores filling the volume of that particular voxel. Denser
185 material appears brighter, voids are black. The local density is controlled by the respective volume
186 fractions of clay content, porosity and non-clay minerals.

187 The chemical and mineralogical composition of some tested specimens (HP3_1, HP3_4,
188 HP3_6, Timo3 and Timo4, see Table 4) from core 5 and 7, determined by the University of Bern, are
189 presented in Table 1, together with the determination of the average grain density measured by
190 using a helium pycnometer. The carbon (organic and inorganic), nitrogen and sulphur components
191 were determined by means of a CNS analyser, and the mineralogy by means of CNS and X-Ray
192 diffractometer. One observes some variability in the clay content that ranges between 46% (HP3_1,
193 core 7) and 59% (Timo 4, core 5), with an average calcite content around 10% and a quartz content
194 between 22 and 34%. The clay-mineral fraction of the Lausen specimens is then not far from that of
195 the shaly facies at Mt Terri (55 – 80%), with however a larger proportion of quartz (10 – 15% at Mt
196 Terri) and a comparable amount of calcite (8 – 20% carbonate at Mt Terri).

197 The data in Table 1 shows that specimens with more quartz have less clay-minerals, with
198 slightly higher average grain density (above 2.7 Mg/m^3 with quartz percentages above 30% in core
199 7), whereas the average grain density of specimens with quartz percentage smaller than 26% (core
200 5, but also specimen HP3_6 in core 7, that indeed exhibit some variability in this regard) is below
201 2.67 Mg/m^3. Other minerals present in smaller proportion are dolomite/ankerite, siderite, albite, K-
202 Felspar and pyrite.

The physical characteristics of the specimens measured just after opening cores 7 and 5 are presented in Table 2. The initial total suction was determined by using the WP4C chilled mirror hygrometer (Decagon). Core 7 was opened one week after receiving the cores, in November 2015, whereas core 5 was opened four months later (March 2016). The smaller water content of core 5 (w = 4.51%) compared to that of core 7 (w = 4,65%) results in having slightly larger suction (s = 21.2 and 19.7 MPa, respectively).

The porosity and degree of saturation were calculated from carefully measuring the sample volume by using hydrostatic weighing of sample cuts in unflavoured oil (commercial French name Kerdane). The degree of saturation and porosity values are known to be sensitive to the changes in the average grain density ρ_s, that in turn depends on the mineralogical composition. Various values of ρ_s have been adopted in the literature for the Opalinus Clay. Gens et al. (2007) used 2.7 Mg/m^3 for samples at Mt Terri, whereas Bossart and Thury (2008) mentioned an average value of 2.74 Mg/m^3, included between a minimum of 2.7 Mg/m^3 and a maximum of 2.77 Mg/m^3. Ferrari et al. (2016) adopted a value of 2.75 - 2.76 Mg/m^3 for samples from Mt Terri and 2.71 - 2.73 Mg/m^3 for deep samples (around 900 m) from a borehole in Schlattingen (eastern Switzerland).

The effects of changes in grain density ρ_s on the value of the degree of saturation S_r and porosity φ are presented in Table 2. One can observe that the degree of saturation of specimens from core 7 changes between 80.2% with ρ_s equal to 2.75 Mg/m^3 and full saturation (101.9%) for ρ_s = 2.66 Mg/m3 (the S_r value slightly larger than 100% could also indicate that 2.66 Mg/m^3 could somehow under-estimate the ρ_s value). Similarly, S_r values of the sample from core 5 range between 72.9 and 90.9%. Also, porosity ranges between 13.7% and 10.8% for core 7 and 14.5% and 11.7% for core 5. Grain density of five of the used samples in this study was directly measured (He-pycnometer) at the University of Berne, yielding values of 2.67 – 2.69 Mg/m^3 for core 5 and 2.67 – 2.72 Mg/m^3 for core 7. Based on these values, taking an average of 2.68 Mg/m^3 for core 5 and 2.70 Mg/m^3 for core 7, the most plausible values for porosity are around 12 %. The resulting lower

saturation for core 5 in comparison with core 7 is also in agreement with the slightly higher suction. The obtained values of S_r are also comparable to those obtained on the Callovo-Oxfordian claystone, they correspond to satisfactory preservation conditions, with minimised evaporation during in-situ coring, core storage and specimen trimming in the laboratory.

3.3. Specimen preparation and testing

Core sections of about 90 mm height and 100 mm diameter were cut from cores 5 or 7 by using a diamond wire saw in dry conditions. Then, a diamond barrel was used to trim the specimens to the desired 38 mm diameter. The height was subsequently reduced to 76 mm by using a diamond wire saw and a specific cylindrical support aimed at obtaining two parallel ends. All specimens were trimmed with the axis perpendicular to the bedding (like the so-called S specimens tested in Favero et al. 2018 and Wild and Amann 2018a).

The drained triaxial tests were conducted in a triaxial cell with enhanced drainage, recently developed by Belmokhtar et al. (2018) to optimise specimen saturation and drainage. In this system (see Figure 3), drainage is made possible by using two non-woven geotextiles placed around the top and the bottom thirds of a standard triaxial specimen (38 mm in diameter and 76 mm in height), with no connection between them. The geotextiles are respectively connected to the upper and lower porous stones. The system allows satisfactory resaturation of the specimen thanks to having no connection between the upper and lower geotextiles, allowing to force water infiltration into the specimen from the top, bottom and lateral side of the cylindrical specimen, with an optimised drainage length close to 19 mm, the specimen radius (see Belmokhtar et al. 2018 for more details). The geotextiles also allow satisfactory drainage of the saturated specimen. Poroelastic calculations made by Belmokhtar et al. (2018) using the actual flow geometry have shown that an axial strain rate of 6.6×10^{-8} s^{-1} was satisfactory to ensure full drainage during shearing for a permeability of 10^{-20} m^2.

252 In this system (see Figure 3a), high precision in local strain measurements was achieved by
253 ensuring direct contact, through the membrane, between the LVDT stems and the specimen, for
254 both radial and axial strain measurements. Water tightness is ensured by putting a neoprene glue
255 drop on the membrane around the stem. The direct contact between the LVDT and the specimen
256 significantly increased the precision of LVDT measurements that came close to 1 µm, the LVDT
257 resolution (see Belmokhtar et al. 2017).

258 The saturation phase was monitored under stress conditions close to in-situ to minimize
259 possible swelling and damage. To do so, once placed on the cell pedestal, the specimens were
260 loaded, at their initial water content, up to the desired stress, by increasing the cell pressure at
261 constant rate (5 kPa/min), while keeping the ducts and geotextiles dry, so as to avoid any contact
262 with water. After applying vacuum through the ducts to the specimen, porous disks and geotextile,
263 de-aired water was infiltrated. The water used was either pure water (tests HP3-1 to 5 at low stress)
264 or a synthetic water prepared in the lab with the composition provided by Nagra from a chemistry
265 analysis of the Lausen borehole water and given in Table 3 (see Pearson et al. 2003).

266 To avoid any corrosion of the pressure volume controller (PVC) by the synthetic water, an
267 interface cell with a maximum admissible fluid pressure of 1.9 MPa was used. The cell was made up
268 of a transparent Plexiglas cylinder with a horizontal flexible neoprene membrane at the middle
269 height, separating the synthetic water from the distilled one coming from the PVC.

270 Saturation was performed while monitoring the change in radial and axial strains, and the end
271 of saturation was assessed once volume changes stabilised. This criterion was adopted by
272 Mohajerani et al. (2012) on a specimen of COx claystone tested in an isotropic compression cell with
273 a 10 mm drainage length. They observed that stabilisation of volume changes occurred after 4 days
274 with B = 0.85, a correct value for saturated COx claystone specimens. In this work, the attempts
275 made to measure the B values were not successful, with too small measured values included
276 between 0.3 and 0.9 (before correction). In all cases, smaller pressures were measured in the upper

277 pressure gauge, because of the larger volume of water contained in the upper drainage system
278 (larger diameter of the ducts). It was suspected that these low *B* values were due to the too low
279 imposed back-pressure (1.9 MPa), not high enough to ensure complete dilution of air in the pore
280 water (Lowe and Johnson 1960, Wu et al. 1997, Wild et al. 2017).

281 The triaxial shear tests were carried out by using two devices, a high pressure triaxial cell
282 (called Timo cell) placed on a 25 tons standard triaxial press with controlled axial strain rate
283 (Wykeham-Farrance), and an autonomous triaxial cell called HP3 (see Hu et al. 2011) in which the
284 axial stress is applied by an hydraulic system driven by a pressure-volume controller (GDS brand),
285 allowing either axial stress or strain controlled testing. In this device (Geodesign brand), there is no
286 effect of the change in confining stress on the axial piston, thanks to an auto-compensating system.
287 In both triaxial devices, the confining stress was applied by means of PVCs. The Timo cell
288 accommodates an internal force gauge of 25 tons maximum, whereas the HP3 cell accommodates
289 an internal force gauge of 2.5 tons maximum, resulting in maximum shear stress of 22 MPa. Tests
290 with confining stress up to 5 MPa were carried out on the HP3 cell, whereas the Timo device was
291 used under larger confining stresses (5, 10 and 15 MPa).

292 Both cells were surrounded by electrical heating belts allowing temperature control, at 25°C
293 in all tests. In cell HP3, two LVDTs were used for axial strain measurement and three for radial strain
294 measurement. In the Timo cell, two LVDTs were used for axial strain measurement and four for
295 radial strain measurements.

296 ## 4. Experimental results

297 The series of drained triaxial tests carried out is presented in Table 4, which shows the stress
298 conditions under which the saturation phase was carried out, the volume increase monitored from
299 the axial and radial displacements measured by the LVDTs during the saturation phase, the effective
300 stress under which the specimen was sheared and the nature of the water (either pure or synthetic

301 water, i.e. a water prepared with the same saline composition as the Opalinus Clay pore water) used
302 to re-saturate the specimen. The tests at low values of confinement (1.3 MPa) and pore water
303 pressure (0.3 MPa) were aimed at mimicking the in-situ stress conditions at around 31 – 37 m in the
304 Lausen borehole.

305 The complete series consisted of 11 tests among which 3 failed, and only the 8 successful tests
306 are presented in the Table. 5 tests were conducted in cell HP3 (HP3-1, 2 and 4 from core 7 and HP3-
307 6 and 7 from core 5) at confining stresses between 1.3 and 6.9 MPa, corresponding to Terzaghi
308 effective stresses σ' of 1 MPa (3 tests), 1.5 MPa (1 test) and 5 MPa. 3 tests (Timo1, 2 and 4) on
309 specimens from core 5 were conducted on the Timo triaxial device at confining stresses between
310 6.9 and 16.9 MPa corresponding to effective stresses of 5, 10 and 15 MPa with a pore water pressure
311 of 1.9 MPa.

312 ### 4.1. Application of confining pressure

313 Figure 4 shows that specimen HP3-7 exhibited after 6 hours a volume decrease of 1.2% when
314 increasing the confining pressure at 1 MPa, at initial water content. One observes that the
315 volumetric strain follows a trend similar to that of the confining pressure. This would not occur in a
316 fully saturated specimen, because the dissipation of excess pore pressure, typical of Terzaghi's
317 consolidation in soils, would result in having a delayed compression. Here, given that the specimen
318 from core 5 is initially not fully saturated, with an initial suction around 20 MPa and a degree of
319 saturation of 86% (see Table 2), the air contained in the specimen can be instantaneously expelled.
320 As a consequence, the increase in stress results in a simultaneous compression of the specimen,
321 with constant water content during compression.

322 ### 4.2. Saturation phase

323 The saturation phase under the target confining pressure was monitored by recording the
324 changes in axial (ε_a) and radial (ε_r) strains with respect to time, together with the volume changes

ε_v ($\varepsilon_v = \varepsilon_a + 2\ \varepsilon_r$) and the water exchanges monitored by the pore water pressure PVC. As an example, Figure 5 shows the saturation phase under 1 MPa of test HP3-1. As in all tests, one observes that the increase in axial strains is larger than in radial ones. Due to the low mean effective stress applied (1 MPa), the volume increase is rather high and equal to 1.73%. In this case, the volumetric strain stabilised rather rapidly, after three days. This test also presented good comparability between the water exchange monitored by the PVC and the volume changes. This was not the case in all tests, and monitored water exchanges were often larger than the volumetric strain, due to both the initial partially saturated state of the samples, and, sometimes, to some micro-leaks. The Figure also presents the data of test Timo4 under σ' = 5 MPa, with a maximum volume increase of 0.43% reached after 15 days. A reasonable correspondence with the water exchange curve is also observed.

The maximum volumetric strains reached at stabilization (Table 4) are presented in Figure 6 with respect to the effective stress applied. They are comparable for tests at 1 MPa effective stress (between 1.13 and 1.74% with a mean value of 1.4%) and they regularly decrease with increased effective stress, with values of 0.34% (Timo2) and 0.43% (Timo4) under 5 MPa and a small value of 0.07% under 15 MPa.

4.3. Shear tests

All drained shear tests were carried out at a controlled strain rate of $6.6 \times 10^{-8}\ s^{-1}$ corresponding to an axial displacement rate 0.3 µm/min, slow enough to ensure good drainage of the specimen with a 19 mm drainage length (Belmokhtar et al. 2018). Results are shown in Figure 7 in terms of changes in shear stress ($q = \sigma_1 - \sigma_3$) with respect to axial strain (ε_1), radial strain (ε_3) and volumetric strain ($\varepsilon_1 + 2\varepsilon_3$). The larger axial strains measured from the external LVDT are also plotted. The numbering from *a* to *h* is done with respect to the applied confining stress, in order to compare more easily similar tests.

Looking at Figure 7a and b, one can observe a good repeatability of tests HP3-1 and HP3-2 carried out under an in-situ Terzaghi effective stress σ' of 1 MPa ($\sigma' = \sigma - u_w$, with $\sigma = 1.3$ MPa, $u_w = 0.3$ MPa), with peak strengths at 8.6 MPa and 9.1 MPa, respectively. The peak strength at 5.4 MPa in test HP3-7 (Figure 7c) under in-situ effective stress is lower than that of HP3-1 and HP3-2. Young's moduli, measured in all tests from first loading at an axial strain of 0.1%, are more or less comparable, with values between 820 MPa and 960 MPa (see Table 5).

Poisson ratios ν_{13} calculated as $\varepsilon_3/\varepsilon_1$ are taken from an average of the 3 (HP3) or 4 (Timo) radial LVDT measurements at 0.1% in axial strain along first loading, with values between 0.08 (HP3-4) and 0.28 (HP3-7) (see Figure 8). Two values at 1 MPa are comparable (0.1 – 0.13 for HP3-1 and HP3-2, respectively) whereas the third one is larger (0.21). The smallest one (0.08) under 1.5 MPa is somewhat low, the two values under 5 MPa (0.16 and 0.19) are in reasonable agreement. It seems that there is an increasing trend with respect to stress with the largest value (0.28) obtained under 15 MPa.

The peak strength in test HP3-4 is equal to 12.5 MPa under 1.5 in-situ stress ($\sigma = 1.8$ MPa, $u_w = 0.3$ MPa) with a Young's modulus $E_1 = 1.18$ GPa. A contracting-dilating behaviour is observed from the changes in volumetric strain around 10 MPa.

Both tests HP3-6 and Timo4 were carried out under 5 MPa effective stress, but under confining pressures of 6.9 MPa and 8.9 MPa and pore water pressures of 1.9 MPa and 3.9 MPa, respectively. Peak strengths are comparable (17.9 MPa and 18.4 MPa, respectively), showing good repeatability in tests carried out in two different devices. Measured Young's modulus are equal to 2.15 GPa and 1.89 GPa in HP3-6 and Timo4, respectively. Test HP3-6 only exhibits a contracting response up to failure, whereas a contracting-dilating behaviour is observed in test Timo4 with transition observed at around 15 MPa shear stress. The test of Figure 7g under 10 MPa effective stress (Timo1) also exhibits a contracting-dilating response, with a peak stress value of 26.6 MPa and an estimated Young modulus $E_1 = 3.97$ GPa. Test Timo3, carried out under 15 MPa

effective stress (Figure 7h) provides a peak stress of 31 MPa, a Young's modulus of 5.77 GPa, with a contracting response.

All Young's moduli are plotted together in Figure 9 with respect to the effective confining stress, showing a linear increase with effective stress, and a good comparability between tests carried out at same confining stresses. Table 5 summarizes all the parameters obtained from the drained shear tests.

The photos of the sheared specimens are presented in Figure 10. One observes that failure occurred with an inclination of around 60° $\pm$ 1° in most samples. Specimen HP3-1 was completely broken along the failure plane because of uncontrolled displacement of the piston. Specimen HP3-2 had the same kind of failure plane, but was also broken into two parts along a plane parallel to the bedding plane, that could correspond to a pre-existing crack. This could explain why the measured Young modulus (E_1 = 820 MPa) is the smallest one under 1 MPa mean effective stress. Comparable inclined failure planes are observed in tests HP3-4 and Timo1.

Figure 11 shows the peak stresses in a q-p' plane (where $p' = p - u_w$ is the Terzaghi mean effective stress and $q = \sigma_1 - \sigma_3$). Discarding the weakest point of test HP3-7, the peak stresses can be fitted by a non-linear curve, that will be further commented in the Discussion section.

5. Discussion

The series of drained triaxial tests presented in this work allows to complement the data base on the mechanical properties of the Opalinus Clay from Lausen in close link with the data from the undrained tests carried out by Giger et al. (2018). The data from drained tests by Favero et al. (2018) and Wild and Amann (2018a) on deep specimens from the shaly facies from the Mt Terri URL (Bossard and Thury 2008) were also considered. At this depth, the stress state is characterised by σ_1 = 6 – 7 MPa, σ_2 = 4 – 5 MPa, and σ_3 = 2 – 3 MPa, with a pore water pressure between 1 and 2 MPa (Martin and Lanyon 2003). The average mean effective stress is around 3 MPa, compared to the 1

398 MPa value estimated at Lausen. On specimens with axis perpendicular to bedding (S-specimens),
399 the effective confining stresses applied by Favero et al. (2018) in their drained tests were equal to
400 2, 5 and 12 MPa, whereas the total confining stresses applied by Wild and Amann (2018) in their
401 undrained tests were 3.09, 4.09 and 6.09 MPa.

402 In swelling claystones, saturation prior to testing results in some increase in volume, even
403 when conducted under stress states close to in-situ (Monfared et al. 2011), or somewhat larger
404 (Mohajerani et al. 2011). Menaceur et al. (2015) and Belmokhtar et al. (2018) measured values
405 between 0.9 and 1% on COx specimens under a mean effective stress of 8 MPa. This feature was
406 further characterized in this work on Opalinus Clay with the data of Figure 6, that show that a
407 confining stress of 15 MPa reduces the volume increase down to 0.07%, with 0.43% under 5 MPa
408 (given the 1 µm accuracy of the LVDT measurements of axial strain ε_a and radial strain ε_r, the
409 uncertainty in volume change $\varepsilon_v = \varepsilon_a + 2\varepsilon_r$ – is 1.2×10^{-4}).

410 This volume increase under hydration has been investigated in more detail through suction
411 controlled tests (with no stress applied) by Wan et al. (2013) and Menaceur et al. (2016b) on the
412 COx claystone, a clay rock comparable to the Opalinus Clay, and by Ferrari et al. (2014) on Opalinus
413 Clay samples from Mt Terri. In all cases, an almost constant volume was observed between the initial
414 suction of the specimens (between 10 and 20 MPa) and a suction of 9 MPa. This was related by
415 Menaceur et al. (2016b) to the stability, in this suction range, of the 2W hydration state of the COx
416 claystone. In other words, it has been demonstrated that the hydration of the COx claystone in this
417 suction range was characterised by the adsorption of two layers of water molecules along the
418 montmorillonite minerals, extending to swelling claystones earlier findings on the adsorption of
419 water along montmorillonite minerals (e.g. Mooney et al. 1952, Ferrage et al. 2005). At suction
420 below 9 MPa, Menaceur et al. (2016b) showed through mercury intrusion porosimetry tests that
421 the significant swelling observed was linked to the developments of cracks, that were also observed
422 in scanning electron microscope by Menaceur (2014) and Delage and Tessier (2020). The increase

423 in volume due to hydration was also investigated at microstructure level by Bornert et al. (2010) by
424 means of Digital Image Correlation. They also observed that a significant part of hydration swelling
425 occurred through the developments of cracks in the clay matrix of the COx claystone.

426 The 15 MPa value under which quite a slight swelling is observed is high for the shallow
427 specimens of Opalinus Clay from Lausen, submitted to an estimated mean in-situ effective stress
428 close to 1 MPa (under which swelling between 1.13 and 1.73% was observed). Adopting from the
429 data of Table 2 an average mean density of 2.47 Mg/m^3 and a hydrostatic pore pressure, the 15 MPa
430 stress would roughly correspond to a depth of around 1000 m. There is no site-specific information
431 on the maximum burial depth of Opalinus Clay, but integration of various geological data on the
432 regional scale suggests that approximately 750 to 1050 m of sediments were eroded at the Miocene
433 / Quaternary boundary (Mazurek et al. 2006). This suggests a maximum burial depth of also
434 approximately 1000 m which corresponds to the 15 MPa stress under which a slight volume increase
435 of 0.07% has been observed. The sensitivity in terms of specimen volume changes to the hydration
436 carried out in the laboratory under (much lower) in-situ stress suggests that the long-term geological
437 uplift and unloading of the Opalinus Clay layer didn't significantly affect the mechanical
438 characteristics of the Opalinus Clay (Crisci et al. 2019, Giger et al. 2018). In other words, Opalinus
439 Clay didn't swell significantly during the significant, but very long, unloading sequence from an
440 estimated 1000 m depth to around 30 m, as also confirmed by the value of the bulk wet density of
441 2.47 Mg/m^3, comparable to that of specimens from greater depths (e.g. Bossart and Thury 2008).
442 This means that the diagenetic bonds resulting from the long term supported high stresses and
443 temperatures at great depth have been kept in such a way that the long-term uplift and unloading
444 didn't result in any major hydration and swelling.

445 The approach adopted by Favero et al. (2018) consisted in increasing the confining stress
446 during hydration so as to neutralize swelling. They observed during their test P-2 on a specimen
447 from the shaly facies at Mt Terri submitted to re-saturation that an effective stress of 3.5 MPa was

able to restrain swelling to 0.4%. This stress can be compared with the vertical stress applied in the oedometer by Mohajerani et al. (2011) to neutralize swelling in a COx specimen, comprised between 1.75 MPa (specimen still swelling) and 3.5 MPa (start of compression). Mohajerani et al. (2011) also noted that the stress necessary to neutralize swelling was not an intrinsic characteristic of the claystone, but depended on the degree of saturation (and hence the suction) from which saturation was carried out, the lower the degree of saturation, the higher the suction and, as a consequence, the higher the stress to apply to neutralize swelling. Note also that, interestingly, the 0.4% swelling observed by Favero et al. (2018) under 3.5 MPa is in the same order of magnitude as that given by Figure 6 (0.43% swelling under 5 MPa). Favero et al. (2018)'s approach seems to be valid when the subsequent confining stresses applied during the testing programme are equal or larger than that applied to neutralize swelling, like for their tests under 5 and 12 MPa, whereas some swelling might occur when saturating under smaller confining stresses (2 MPa). Wild and Amann (2018) carried out air flushing and subsequent saturation phase under effective isotropic stresses between 20 and 600 kPa, resulting in a swelling comprised between 0.5 and 1.6% (Wild et al. 2017).

An appropriate way of checking the possible effect of swelling during saturation on the shear strength properties of the Opalinus clay is to compare our data on low depth specimens from Lausen to those of the undrained shear tests of Giger et al. (2018), who also performed two drained tests at 6.4 and 18.4 MPa initial mean effective stress on specimens of 38 mm in height and 19 mm in diameter with side drains (h = 9.5 mm) at a strain rate of 2×10^{-8} s^{-1}. The comparison is presented in Figure 12, in which the black dotted line was drawn from the peak shear stresses from undrained tests (green stress paths). One observes quite a good comparability between our drained tests (strain rate 6.6×10^{-8} s^{-1}) and Giger's undrained tests (strain rate 2×10^{-7} s^{-1}) for stresses larger than 10 MPa, confirming their estimation of friction angle (19°) and cohesion (6.8 MPa). Interestingly, their drained test at 6.4 MPa (in blue) is in quite good agreement with our test at 5 MPa. Their peak stress at p' = 18.4 MPa (in black) is located above the dotted line, in link with the smaller porosity (ϕ

= 10.3% at 18.4 MPa and 13.1% at 6.8 MPa, the latter being slightly larger than the porosity of our specimens, ϕ = 12.3%). The Figure also shows that all the data of drained tests below the 10 MPa effective confining pressure (p' = 6.4 MPa from Giger et al. 2018 in blue stress path, 5 MPa, 1.5 and 1 MPa for our data in red stress paths) are located below the data of the undrained shear tests. Actually, the distance along the drained stress path between the peak stress of our drained tests and the black dotted line drawn from undrained tests increases with respect to the magnitude of the swelling observed in Figure 6, the larger the swelling, the larger the distance.

The data of Figure 12 are now compared (Figure 13) with the peak stresses obtained from drained tests (Favero et al. 2018) and undrained tests (Wild and Amann 2018b) carried out on deep specimens from Mt Terri with axis perpendicular to bedding. In spite of the different origins of the specimens (with larger porosity and some difference in mineralogy), it can be observed that the peak stress at 12 MPa of Favero et al. (2018), in a stress range with no significant swelling upon hydration, is located slightly below the Lausen failure criterion derived from both Giger's undrained tests and our drained tests, in link with the larger porosity of the Mt Terri specimens (17% versus 12% at Lausen). From their peak data, Favero et al. (2018) derived a friction angle of 22° and a cohesion of 2.6 MPa. A good agreement is observed between their drained data at 2 MPa and the undrained ones of Wild and Amann (2018) in the same stress range. The failure points of the undrained tests of Wild and Amman (2018a) exhibit a comparable non-linear shape with respect to our data on Lausen, with a clear departure, in the low stress area, from the straight line obtained from Giger's undrained tests. This non linearity raises the question of the possible consequences of hydration swelling at low stress. It has been shown that swelling in claystones occurs both at the crystalline level within platelets and, as commented earlier, through the development of micro-cracks oriented along the bedding plane (Bornert et al. 2010, Menaceur 2016a, Delage and Tessier 2020). Giger's undrained data, that are not affected by swelling, show a linear shape of the criterion down to a value of p' of 3 MPa, an area where the data of our drained tests on Lausen specimens

provide smaller peak strengths. The question as to whether the micro-cracks resulting from hydration swelling affect the mechanical response of the claystone at low stress then arises. As a consequence, it is difficult to definitely conclude about the shape of the failure criterion at low stresses (non-linear, as observed, or linear, as extrapolated from Giger's data). Further undrained tests at low confinement stresses with no specimen hydration, as done by Giger et al. (2018), would certainly help in further concluding in this regard.

Figure 9 shows the changes in Young moduli (first loading stage) with respect to the confining effective stress of our drained tests. Swelling upon hydration might also have some influence in the estimation of Young's moduli at low stress. The Young's moduli of 4 and 8 GPa obtained under 10 and 15 MPa, respectively, correspond to hydration swelling smaller than 0.2% (Figure 6), in a zone where a good agreement between drained and undrained tests has been observed (Figure 12). A possibility of facing at lower stresses some under-estimation of Young's moduli, in particular under 1 and 1.5 MPa, might be considered. This would question the linearity observed in Figure 9.

The comparison of our Young's moduli with other available data is done in Figure 14, with moduli obtained from first loading in drained tests by Giger et al. (2018) on Lausen specimens, and those from drained stress cycles on Mt Terri specimens by Favero et al. (2018). Giger's data at 6.2 MPa are reasonably comparable with our data, whereas their modulus at 18.4 MPa is smaller than what could be extrapolated from our data. The Young's moduli determined from stress cycles are larger than those from first loading, which is perhaps the reason why Favero's data are slightly larger than the Lausen data, in spite of having in Mt Terri a larger porosity. The change in their values with respect to stress is also linear.

The changes in Poisson coefficient ν_{13} with stress obtained from first loading are presented in Figure 15 and compared to those obtained, from unload-reload cycles, by Giger et al (2018) on same Lausen shallow specimens and Favero et al. (2018) on deep Mt Terri specimens. Given that ν_{13} values are determined by the ratio $\varepsilon_3/\varepsilon_1$, and that swelling results in the development of sub-

horizontal cracks, one can consider that larger values of ε_1 (perpendicular to bedding) could be obtained in samples having exhibited more hydration swelling. Conversely, changes in ε_3 should be less sensitive to swelling. Beside the method of determination (first loading data are smaller than those from stress cycles), this might explain why our Poisson coefficients under low stresses may be under-estimated. This should not occur under higher stress, for which we obtained ν_{13} = 0.19 under 10 MPa and 0.28 under 15 MPa. This last (first loading) value is in good agreement with those of 0.28 and 0.29 obtained from unload-reload cycles by Giger et al. (2018) under 6.4 and 18.4 MPa and Favero et al. (2018) under 2, 5 and 12 MPa. Note that these values are fairly stress independent.

The peak stresses obtained on specimens of the Callovo-Oxfordian claystone from drained tests by Hu et al. (2014), Menaceur et al. (2015) and Belmokhtar et al. (2018) at various porosities between 13 and 17% are now compared in Figure 16 with the data from the Opalinus Clay. Interestingly, the peak stresses of both claystones are in the same range of magnitude. Above 10 MPa, one can draw for the COx claystone two parallel failure lines with respect to the specimen porosity, that compare well with the data of the Opalinus Clay, indicating comparable angles of friction.

The same conclusion can be drawn in terms of Young's moduli. Figure 17 shows satisfactory comparability between both claystones. Again, the apparent linearity below 10 MPa should be further checked. Note that the mean effective stress at 490 m depth in the Bure URL in France is close to 9.5 MPa (major total horizontal stress σ_H = 16.2 MPa, minor total horizontal stress σ_h = 12.4 MPa, vertical total stress σ_v = 12.7 MPa and pore water pressure u_w = 4.7 MPa, see Wileveau et al. 2007; equivalent isotropic Biot *b* coefficient around 0.9, see Belmokhtar et al. 2017). The Young's modulus of Opalinus Clay, found around 5.6 MPa at 15 MPa in a test in which little swelling occurred under hydration (see Figure 6) is perhaps under-estimated at lower stresses.

6. Concluding remarks

The determination of the mechanical properties of swelling claystones is challenging, given their high sensitivity to changes in water content. In this regard, various recent experimental investigations carried out in the triaxial apparatus on Opalinus Clay specimens have recently been published, both in drained and undrained conditions (Wild et al. 2017a, Favero et al. 2018, Wild and Amman 2018, Giger et al. 2018). In this work, the data of the drained triaxial tests carried on saturated shallow Opalinus Clay specimens from Lausen are compared to undrained data obtained by Giger et al. (2018) on specimens from same location and depth (around 30 m). Data are also compared with those obtained by Favero et al. (2018) and Wild and Amman (2018) on deep specimens of the shaly facies of the Mt Terri URL (around 250 m). From these comparisons, various conclusions can be drawn about the relevance of drained triaxial testing in claystones and shales. The data of undrained tests, in which no hydration swelling occurred during the test set-up, indicate a linear shape of the failure criterion of the Lausen specimens, down to an effective confining stress of 3 MPa. The drained tests conducted in this work evidenced an excellent correspondence with undrained data at effective confining stresses larger than 10 MPa, for which no significant swelling (< 0.2 %) was detected upon hydration during the saturation phase (conducted under the same confining stress as that adopted for shearing). Conversely, a departure from linearity was observed at lower effective confining stresses, in an area where some swelling was observed under hydration (from 0.4% under 5 MPa and up to 1.3 – 1.7 % under 1 MPa). A similar non-linear shape of the failure criterion at low stresses has also been observed by Wild and Amman (2018a) and Favero et al. (2018). The question as to whether this swelling at lower stresses tends to provide an under-estimation of the peak failure data is discussed, and it is suggested that undrained tests at low initial effective confining stress would be necessary to investigate whether the linear failure criterion evidenced by Giger et al. (2018) might be extended at low stresses, of whether the failure criterion is really non-linear at low stresses, as observed from drained tests data. This would mean that there

571 is no effect of hydration swelling at low stresses. The same question is raised with respect to the
572 changes in Young moduli with stress, that have been observed as being linear, even at low confining
573 stresses. If the micro-cracks oriented along the bedding plane resulting from swelling under
574 hydration had some effects, they would result in providing under-estimated values of Young moduli
575 in specimens having their axis perpendicular to bedding, due to the closing of micro-cracks during
576 the increase in mean stress during shearing. The same would actually hold for the determination of
577 the Poisson ratio at small stresses, due to over-estimation of axial strain.

578 Interestingly, the mechanical properties of the Opalinus Clay are comparable to those of the
579 Callovo-Oxfordian claystone, a possible host-rock in France that has a comparable mineralogical
580 composition. This holds for both peak strengths and Young' moduli, with a friction angle comparable
581 to that of Opalinus Clay. Data obtained below 10 MPa might be under-estimated for the same
582 reason.

583

584 Further experimental investigations by undrained triaxial tests at low confining stresses
585 appears then necessary to get a more detail insight in the shape of the failure criterion of these
586 swelling claystones at low stress.

587 ## 7. Acknowledgements

588 The work presented in this paper was supported by the Swiss National Cooperative for the
589 Disposal of Radioactive Waste (Nagra) as part of the second author's PhD thesis (Belmokhtar 2017).
590 Nagra also provided the Opalinus Clay specimens, their X-Ray tomographic investigation and
591 mineralogical determination. The authors are deeply grateful to Dr. Silvio Giger for providing the
592 samples, for the detailed and helpful discussions about the experimental program, the analysis of
593 test data and for his detailed and sound comments that definitely helped improving the manuscript.

8. References

Andra (2005) Synthesis argile: evaluation of the feasibility of a geological repository in argillaceous formation.

Aoki T, Tan CP, Cox RHT, Bamford WE (1995) Determination ofanisotropic poroelastic parameters of a transversely isotropic shale by means of consolidated undrained triaxial tests. Proc. 8th Int. Cong. Rock Mech. T. Jujii Ed, Tokyo, Japan, 2, 172-176.

Belmokhtar M. (2017). Contributions à l'étude du comportement thermo-hydro-mécanique de l'argilite du Callovo-Oxfordien (France) et de l'Argile à Opalinus (Suisse). PhD thesis, Ecole des Ponts ParisTech – Université Paris-Est (in French).

Belmokhtar M, Delage P, Ghabezloo S, Menaceur H, Tang AM, Conil N (2017) Poroelasticity of the Callovo–Oxfordian Claystone. Rock Mech Rock Eng 50:871–889. doi: 10.1007/s00603-016-1137-3

Belmokhtar M., Delage P., Ghabezloo S. and Conil N. (2018). Drained triaxial tests in low permeability shales. Application to the Callovo-Oxfordian claystone. *Rock Mechanics and Rock Engineering* 51(7), 1979-1993, doi: 10.1007/s00603-018-1442-0.

Bishop AW, Henkel DJ (1957) The measurement of soil properties in the triaxial test. Edward Arnold (Publishers) LTD, London

Blight GE (1963) The effect of nonuniform pore pressures on laboratory measurements of the shear strength of soils. Symposium on laboratory shear testing of soils, ASTM STP 361, 173 – 184.

Bonini M, Debernardi D, Barla M, Barla G (2009) The Mechanical Behaviour of Clay Shales and implications on the Design of Tunnels. Rock Mech Rock Eng 42(2): 361-388.

Bock H (2009) RA experiment: updated review of the rock mechanics properties of the Opalinus clay of the Mont Terri URL based on laboratory and field testing. Technical report.

Bornert M, Valès F, Gharbi H, Nguyen Minh D (2010) Multiscale Full-Field Strain Measurements for Micromechanical Investigations of the Hydromechanical Behaviour of Clayey Rocks. Strain 46, 33–46.

Bossart P (2011) Characteristics of the Opalinus Clay at Mont Terri. http://www.mont-terri.ch/internet/mont-terri/de/home/geology/ key_characteristics.html.

Bossart P, Thury, M., (2008) Mont Terri Rock laboratory –Project, Programme 1996 to 2007 and results. Reports of the Swiss geological survey No. 3 –Swiss geological survey, Wabern.

Busch A, Alles S, Gensterblum Y, Prinz D, Dewhurst D, Raven M, et al. (2008) Carbon dioxide storage potential of shales. Int J. Greenh Gas Control 2(3):297–308.

Charlier R, Collin F, Pardoen B, Talandier J, Radu JP, Gerard P (2013) An unsaturated hydro-mechanical modelling of two in-situ experiments in Callovo-Oxfordian argillite. Eng Geol 165:46–63.

Chiarelli AS (2000) Étude expérimentale et modélisation du comportement mécanique de l'argilite de l'est. PhD thesis, Université Lille I.

Chiarelli AS, Shao JF, Hoteit N (2003) Modeling of elastoplastic damage behavior of a claystone. Int J Plast 19:23–45.

Chiu HK, Johnston IW, Donald IB (1983) Appropriate Techniques for Triaxial Testing of Saturated Soft Rock. Int J Rock Mech Mining Sc & Geomech Abst 20(3):107-120.

636 Corkum AG, Martin CD (2007) The mechanical behaviour of weak mudstone (Opalinus Clay) at low
637 stresses. Int J Rock Mech Min Sci 44(2):196–209

638 Coussy O (2007) Revisiting the constitutive equations of unsaturated porous solids using a
639 Lagrangian saturation concept. 1675–1694.

640 Crisci E, Ferrari A, Giger S, Laloui L (2019) Hydro-mechanical behaviour of shallow Opalinus Clay
641 shale. Engineering Geology (251), 214 – 227.

642 Davy CA, Skoczylas F, Barnichon JD, Lebon P (2007) Permeability of macro-cracked argillite under
643 confinement: Gas and water testing. Phys Chem Earth, Parts A/B/C 32:667–680.

644 Delage P, Cui YJ, Tang AM (2010) Clays in radioactive waste disposal. J Rock Mech Geotech Eng
645 2:111–123. doi: 10.3724/SP.J.1235.2010.00111

646 Delage P, Menaceur H, Tang AM, Talandier J (2014) Suction effects in deep Callovo-Oxfordian
647 claystone Suction effects in deep Callovo-Oxfordian claystone. Géotechnique Lett 4:267–271.

648 Delage P., Tessier D. 2020. Macroscopic effects of nano and microscopic phenomena in clayey soils and
649 clay rocks. *Geomechanics for Energy and the Environment*, doi:10.1016/j.gete.2019.100177.

650 Douma, L.A., Dautriat, J., Sarout, J., Dewhurst, D.N. and Barnhoorn, A., 2020. Impact of water saturation
651 on the elastic anisotropy of the Whitby Mudstone, United Kingdom. Geophysics, 85(1), pp.MR57-
652 MR72.

653 Detournay E, Cheng AH (1993) Fundamentals of Poroelasticity. Chapter 5 Compr Rock Eng Princ
654 Pract Proj Vol II, Anal Des Method, ed C Fairhurst, Pergamon Press II:113–171.

655 Einstein HH (2000) Tunnels in Opalinus Clayshale: A Review of Case Histories and New
656 Developments. Tunnelling and underground space technology 15(1): 13-29.

657 Escoffier S (2002) Caractérisation expérimentale du comportement hydromécanique des argilites
658 de Meuse Haute-Marne. PhD thesis, Institut National Polytechnique de Lorraine.

659 Eseme E, Urai JL, Krooss BM, Littke R (2007) Review of mechanical properties of oil shales:
660 implications for exploitation and basin modelling. Oil Shale 24(2):159–174

661 Ewy RT, Stankovich RJ, Bovberg CA (2003) Mechanical Behavior of Some Clays and Shales from
662 200m to 3800m Depth. In: Culligan P, Einstein H, Whittle A (eds) Soil and Rock America 2003:
663 Proc. 12th PanAm Conf Soil Mech Geotech Eng and 39th US Rock Mech Symp. Verlag Glückauf,
664 Essen, 445-452.

665 Ewy RT (2015) Shale/claystone response to air and liquid exposure, and implications for handling,
666 sampling and testing. Int J Rock Mech Min Sci 80:388–401.

667 Ewy RT (2018) Practical approaches for addressing shale testing challenges associated with
668 permeability, capillarity and brine interactions. Geomech Energy Environ.
669 http://dx.doi.org/10.1016/j.gete.2018.01.001.

670 Favero V, Ferrari A, Laloui L. (2018) Anisotropic behaviour of Opalinus Clay through consolidated
671 and drained triaxial testing in saturated conditions. Rock Mech Rock Eng. 51(5): 1305 – 1319.

672 Ferfera FMR (2001) Mécanismes physiques de l'évolution de la perméabilité d'un grès sous
673 chargements simulant la déplétion d'un gisement. Oil Gas Sci Technol 56:347–355. doi:
674 10.2516/ogst:2001030

675 Ferrage E, Lanson B, Sakharov BA, Drits VA (2005) Investigation of smectite hydration properties
676 by modeling experimental X-ray diffraction patterns: part I. Montmorillonite hydration
677 properties. Am Mineral 90: 1358–1374.

678 Gaucher E, Robelin C, Matray JM, Négrel G, Gros Y, Heitz JF, Vinsot A, Rebours H, Cassagnabère A,

679 Bouchet A (2004) ANDRA underground research laboratory: Interpretation of the
680 mineralogical and geochemical data acquired in the Callovian-Oxfordian formation by
681 investigative drilling. Phys Chem Earth 29:55–77.

682 Gens A, Vaunat J, Garitte B, Wileveau Y (2007) In situ behaviour of a stiff layered clay subject to
683 thermal loading : observations and interpretation. Géotechnique 57:207–228.

684 Ghabezloo S, Sulem J, Guédon S, Martineau F, Saint-Marc J (2008) Poromechanical behaviour of
685 hardened cement paste under isotropic loading. Cem Concr Res 38:1424–1437.

686 Ghabezloo S, Sulem J (2009) Stress dependent thermal pressurization of a fluid-saturated rock.
687 Rock Mech Rock Eng 42:1–24.

688 Ghabezloo S, Sulem J (2010) Effect of the volume of the drainage system on the measurement of
689 undrained thermo-poro-elastic parameters, Int. J. Rock Mech. Min. Sci., 47, 60–68.

690 Gibson RE, Henkel DJ (1954) Influence of Duration of tests at Constant Rate of Strain on Measured
691 “Drained” Strength. Géotechnique 4:6–15.

692 Giger S, Ewy RT, Favero V, Stankovic R, Keller LM (2018) Consolidated-undrained triaxial testing of
693 Opalinus Clay: Results and method validation. Geomech Energy Environ 14, 16 – 28.

694 Hecht F (2012) New development in freefem+. J Numer Math 20:251–265. doi: 10.1515/jnum-
695 2012-0013

696 Hu DW, Zhang F, Shao JF (2014) Experimental study of poromechanical behavior of saturated
697 claystone under triaxial compression. Acta Geotech 9:207–214.

698 Islam MA, Skalle P (2013) An experimental investigation of shale mechanical properties through
699 drained and undrained test mechanisms. Rock Mech Rock Eng 46:1391–1413. doi:
700 10.1007/s00603-013-0377-8

701 ISRM, 1979. Suggested methods for determining water content, porosity, density, absorption and
702 related properties and swelling and slake-durability index properties. Int. J. Rock Mech. Min.
703 Sci. Geomech. Abstr. 16 (2), 141–156.

704 Klinkenberg M, Kaufhold S, Dohrmann R, Siegesmund S (2009). Influence of carbonate
705 microfabrics on the failure strength of claystones. Eng Geol 107: 42 - 54.

706 Martin CD, Lanyon GW (2003) Measurement of in-situ stress in weak rocks at Mont Terri rock
707 laboratory, Switzerland. Int. J. Rock Mech. Min. Sci. 40, 1077–1088.

708 Masri M, Sibai M, Shao JF, Mainguy M (2014) Experimental investigation of the effect of
709 temperature on the mechanical behavior of Tournemire shale. Int J Rock Mech Min Sci
710 70:185–191.

711 Mazurek M, Gautschi A, Marschall P, Vigneron G, Lebon P, Delay J. (2008) Transferability of
712 geoscientific information from various sources (study sites, underground rock laboratories,
713 natural analogues) to support safety cases for radioactive waste repositories in argillaceous
714 formations. Phys Chem Earth 33 (suppl 1): S95–S105.

715 Menaceur H (2014) Comportement Thermo-Hydro-Mécanique Et Microstructure de L’Argilite Du
716 Callovo-Oxfordien. PhD thesis, Ecole des Ponts ParisTech - Université Paris Est (in French).

717 Menaceur H, Delage P, Tang A-M, Conil N (2015) The thermo-mechanical behaviour of the Callovo-
718 Oxfordian claystone. Int J Rock Mech Min Sci 78:290–303.

719 Menaceur H, Delage P, Tang A-M, Conil N (2016a) On the Thermo-Hydro-Mechanical Behaviour of
720 a Sheared Callovo-Oxfordian Claystone Specimen with Respect to the EDZ Behaviour. Rock
721 Mech Rock Eng 49:1875–1888.

722 Menaceur H., Delage P., Tang A.M. and Talandier J. 2016b. The status of water in swelling shales:
723 an insight from the water retention properties of the Callovo-Oxfordian claystone. Rock Mech
724 Rock Eng 49 (12), 4571- 4586

725 Mohajerani M, Delage P, Monfared M, Tang A-M, Sulem J, Gatmiri B (2011) Oedometric
726 compression and swelling behaviour of the Callovo-Oxfordian argillite. Int J Rock Mech Min
727 Sci 48:606–615.

728 Mohajerani M, Delage P, Sulem J, Monfared M, Tang A-M, Gatmiri B (2012) A laboratory
729 investigation of thermally induced pore pressures in the Callovo-Oxfordian claystone. Int J
730 Rock Mech Min Sci 52:112–121.

731 Mohajerani M, Delage P, Sulem J, Monfared M, Tang A-M, Gatmiri B (2013) The Thermal Volume
732 Changes of the Callovo–Oxfordian Claystone. Rock Mech Rock Eng 47:131–142.

733 Monfared M (2011) Couplages température-endommagement-perméabilité dans les sols et roches
734 argileux. PhD thesis, Ecole des ponts ParisTech - Université Paris-Est.

735 Monfared M, Delage P, Sulem J, Mohajerani M, Tang A-M, De Laure E (2011a) A new hollow
736 cylinder triaxial cell to study the behavior of geo-materials with low permeability. Int J Rock
737 Mech Min Sci 48:637–649.

738 Monfared M, Sulem J, Delage P, Mohajerani M (2011b) A Laboratory Investigation on Thermal
739 Properties of the Opalinus Claystone. Rock Mech Rock Eng 44:735–747. doi: 10.1007/s00603-
740 011-0171-4.

741 Mooney RW, Keenan AC, Wood LA (1952) Adsorption of water vapor by montmorillonite. II. Effect
742 of exchangeable ions and lattice swelling as measured from X-ray diffraction. J Am Chem Soc
743 74:1371–1374.

744 Nadri, D., Sarout, J., Bóna, A. and Dewhurst, D., 2012. Estimation of the anisotropy parameters of
745 transversely isotropic shales with a tilted symmetry axis. Geophysical Journal International,
746 190(2), 1197-1203.

747 Nakase A and Kamei T (1986) Influence of strain rate on undrained shear characteristics of K0-
748 consolidated cohesive soils. Soils and Foundations 26 (1), 85 – 95.

749 Naumann M, Hunsche U, Schulze O (2007) Experimental investigations on anisotropy in dilatancy,
750 failure and creep of Opalinus Clay. Phys Chem Earth 32:889–895. doi:
751 10.1016/j.pce.2005.04.006.

752 Pearson FJ, Arcos D, Bath A, Boisson JY, Fernandez AM, Gäbler HE, Gaucher E, Gautschi, A, Griffault
753 L, Hernan P, Waber N (2003) Geochemistry of Water in the Opalinus Clay Formation at the
754 Mont Terri Rock Laboratory. Synthesis Report. Geology Series, No. 5 Swiss Federal Office for
755 Water and Geology, Bern, Switzerland.

756 Pham QT, Vales F, Malinsky L, Nguyen M-D, Gharbi H (2007) Effects of desaturation–resaturation
757 on mudstone. Phys Chem Earth, Parts A/B/C 32:646–655.

758 Bornert M, Valès F, Gharbi H, Nguyen Minh D (2010) Multiscale full-field strain measurements for
759 micromechanical investigations of the hydromechanical behaviour of clayey rocks. Strain 46:33–46.
760 https://doi.org/10.1111/j.1475-1305.2008.00590.x

761 Sarout J, Detournay E (2011) Chemoporoelastic analysis and experimental validation of the pore pressure
762 transmission test for reactive shales. Int J Rock Mech Min Sci 48:759–772.
763 https://doi.org/10.1016/j.ijrmms.2011.04.009

764 Schmitt L, Forsans T, Santarelli FJ (1994) Shale Testing and Capillary Phenomena, Int J Rock Mech Mining Sc
765 & Geomech Abst, 31(5): 411-427.

766 Skempton A (1954) The pore-pressure coefficients A and B, Géotechnique 4(4): 143–147.

767 Steiger RR, Leung RK 1991. Consolidated undrained triaxial test procedure for shales. Rock
768 mechanics as a Multidisplinary Science, Proc. 32nd U.S. Syrup., JC Roegiers Ed: 637-646.

769 Spang B (2002) Excel add-in for properties of water and steam in SI units.
770 http://www.cheresources.com/iapwsif97.shtml.

771 Swan G, Cook J, Bruce S, Meehan R (1989) Strain rate effects in Kimmeridge bay shale. Int. J. Rock
772 Mech. Min. Sci. & Geomech. Abstr, 26(2): 135-149.

773 Terzaghi, K., & Fröhlich, O. K. (1936). Theorie der Setzung von Tonschichten. Wien, Franz Deuticke:
774 Leipzig.

775 Thury M, Bossart P (1999). Results of the hydrogeological, geochemical and geotechnical
776 experiments performed in the Opalinus Clay (1996 - 1997). Geol report 23. Swiss Geological
777 Survey.

778 Valès F, Nguyen Minh D, Gharbi H, Rejeb A (2004) Experimental study of the influence of the
779 degree of saturation on physical and mechanical properties in Tournemire shale (France).
780 Appl Clay Sci 26:197–207.

781 Villamor-Lora R, Ghazanfari E, Asanza Izquierdo E (2016) Geomechanical Characterization of
782 Marcellus Shale. Rock Mech Rock Eng, 49(9), 3403–3424.

783 Wan M, Delage P, Tang A-M, Talandier J (2013) Water retention properties of the Callovo-
784 Oxfordian claystone. Int J Rock Mech Min Sci 64:96–104.

785 Wang L, Bornert M, Chanchole S (2013) Micro-scale experimental investigation of deformation and
786 damage of argillaceous rocks under hydric and mechanical loads. Poromochanics V ASCE
787 1635–43.

788 Wild KM, Barla M, Turinetti G, Amann F (2017) A multi-stage triaxial testing procedure for low
789 permeable geomaterials applied to Opalinus Clay. J Rock Mech Geotech Eng. 9: 519–530.

790 Wild KM and Amann F (2018a) Experimental study of the hydro-mechanical response of Opalinus
791 Clay – Part 1: Pore pressure response and effective geomechanical properties under
792 consideration of confinement and anisotropy. Eng Geol 237: 32–41.

793 Wild KM and Amann F (2018b) Experimental study of the hydro-mechanical response of Opalinus
794 Clay – Part 2: Influence of the stress path on the pore pressure response. Eng Geol 237: 92 –
795 101.

796 Wileveau Y, Cornet FH, Desroches J, Blumling P (2007) Complete in situ stress determination in an
797 argillite sedimentary formation. Phys Chem Earth 32:866–878. doi:
798 https://doi.org/10.1016/j.pce.2006.03.018

799 Wissa AEZ (1969) Pore pressure measurement in saturated stiff soils. J. Soil Mech. Fdns Div. Am.
800 Soc. civ. Engrs 95:SM4, 1063-1073.

801 Wu B, Tan CP, Aoki T (1997) Specially designed techniques for conducting consolidated undrained
802 triaxial tests on low permeability shales. Int J Rock Mech Min Sci 34:336.e1-336.e14. doi:
803 10.1016/S1365-1609(97)00168-8

804 Yven B, Sammartino S, Geraud Y, Homand F, Villieras F (2007) Mineralogy, texture and porosity of
805 Callovo-Oxfordian argilites of the Meuse/Haute-Marne region (eastern Paris Basin).
806 Mémoires la société Géologique Fr 0249–7546:73–90.

807 Zhang CL (2011) Experimental evidence for self-sealing of fractures in claystone. Phys Chem Earth
808 36:1972–1980.

809 Zhang CL, Rothfuchs T (2004) Experimental study of the hydro-mechanical behaviour of the
810 Callovo-Oxfordian argillite. Appl Clay Sci 26:325–336.

811 Zhang CL, Rothfuchs T, Su K, Hoteit N (2007) Experimental study of the thermo-hydro-mechanical
812 behaviour of indurated clays. Phys Chem Earth, Parts A/B/C 32:957–965.

813 Zhang F, Xie SY, Hu DW, Gatmiri B (2012) Effect of water content and structural anisotropy on
814 mechanical property of claystone. Appl Clay Sci 69:79–86.

815

816

817

818 **List of Tables**

825

826

827 **List of Figures**

868

869 *Table 1. Chemical and mineralogical composition of some tested specimens from both cores (values provided by the*

870 *University of Bern).*

		CNS analyser				**Mineralogy (XRD + CNS)**									**Grain density**	
Core	Specimen	Organic Carbon [wt.%]	Inorganic Carbon [wt.%]	Sulphur [wt.%]	Nitrogen [wt.%]	Calcite [wt.%]	Dolomite / Ankerite [wt.%]	Siderite [wt.%]	Quartz [wt.%]	Albite [wt.%]	K-feldspar [wt.%]	Pyrite [wt.%]	Organic Carbon [wt.%]	Total clay minerals [wt.%]	Grain density [Mg/m^3]	Error [Mg/m^3]
7	HP3_1	0.61	1.42	1.56	0.05	9	1.7	0.7	34	3	2	2.9	0.6	46	2.716	0.002
7	HP3_4	0.65	2.14	0.33	0.06	13	3	1.5	30	1.3	2	0.6	0.7	48	2.704	0.002
7	HP3_6	1.03	1.52	0.14	0.09	10	1.5	1.2	25	2	2	0.3	1.0	57	2.671	0.001
5	Timo3	1.10	1.55	0.42	0.09	11	1.5	0.8	26	2	2	0.8	1.1	55	2.669	0.001
5	Timo4	0.96	1.69	0.69	0.09	12	1.3	0.6	22	1.2	1.6	1.3	1.0	59	2.690	0.001

871

872

873 *Table 2. Characteristics of the specimens extracted from core 5 and 7, measured on sample cuts at core opening.*
874

Core	Depth interval (m below ground level)	*w* (%) Core opening ± 0.05	ρ (Mg/m^3) ± 0.03	ρ_d (Mg/m^3) ± 0.03	Suction (MPa) ± 0.5	ρ_s (Mg/m^3) ± 0.03	Porosity ϕ (%) ± 0.1	Degree of saturation S_r (%) ± 2
7	36.4 37.2	4.65	2.48	2.372	19.7	2.75	13.7	80.2
						2.72	12.8	86.2
						2.7	**12.1**	**90.8**
						2.68	11.5	96.0
						2.66	10.8	101.9
5	30.4 31.4	4.51	2.46	2.35	21.2	2.75	14.5	72.9
						2.72	13.6	77.9
						2.7	13.0	81.8
						2.68	**12.3**	**86.0**
						2.66	11.7	90.9

875

876

877 *Table 3. Composition of synthetic pore water*

	NaCl	$NaHCO_3$	$CaCl_2$ $2H_2O$	KCl	$MgCl_2$ $6H_2O$	Na_2SO_4
Concentration [mg/l H2O]	2.25	0.01	0.58	0.06	0.62	1.14

878

879

880 *Table 4. Drained triaxial tests (all specimens with axis perpendicular to bedding)*

Test	Core	Saturation				Shearing stress conditions			Water
		σ (MPa) ± 0.01	u (MPa) ± 0.01	σ' (MPa) ± 0.01	Volume increase (%) ± 0.01	σ (MPa) ± 0.01	u (MPa) ± 0.01	σ' (MPa) ± 0.01	
HP3-1	7	1.3	0.3	1	1.73	1.3	0.3	1	Demineralised
HP3-2	7	1.3	0.3	1	1.63	1.3	0.3	1	Demineralised
HP3-4	7	1.3	0.3	1	1.15	1.8	0.3	1.5	Demineralised
HP3-6	5	6.9	1.9	5	No monitoring	6.9	1.9	5	Pearson
HP3-7	5	2.9	1.9	1	1.27	2.9	1.9	1	Pearson
Timo1	5	11.9	1.9	10	No monitoring	11.9	1.9	10	Pearson
Timo3	5	16.9	1.9	15	0.07	16.9	1.9	15	Pearson
Timo4	5	6.9	1.9	5	0.43	6.9	1.9	5	Pearson

881

882

883 *Table 5. Measured parameters from the drained triaxial shear tests. All tests carried out at 6.6 x $10^{-8}s^{-1}$*

Test	σ (MPa) ± 0.01	u (MPa) ± 0.01	σ' (MPa) ± 0.01	q_{max} (MPa) ± 0.01	ε_a peak ± 0.01	E_1 (GPa) ± 0.05	v_{12} (-) ± 0.01
HP3-1	1.3	0.3	1.0	8.6	0.77	0.9	0.13
HP3-2				9.1	1.12	0.82	0.10
HP3-7	2.9	1.9		5.4	0.78	0.96	0.21
HP3-4	1.8	0.3	1.5	12.5	0.76	1.18	0.08
HP3-6	6.9	1.9	5	17.9	2.25	2.15	0.19
Timo4	8.9	3.9		18.4	1.36	1.89	0.16
Timo1	11.9	1.9	10	26.6	1.10	3.97	0.19
Timo3	16.9	1.9	15	31	1.60	5.77	0.28

884

885

886

887

888

889

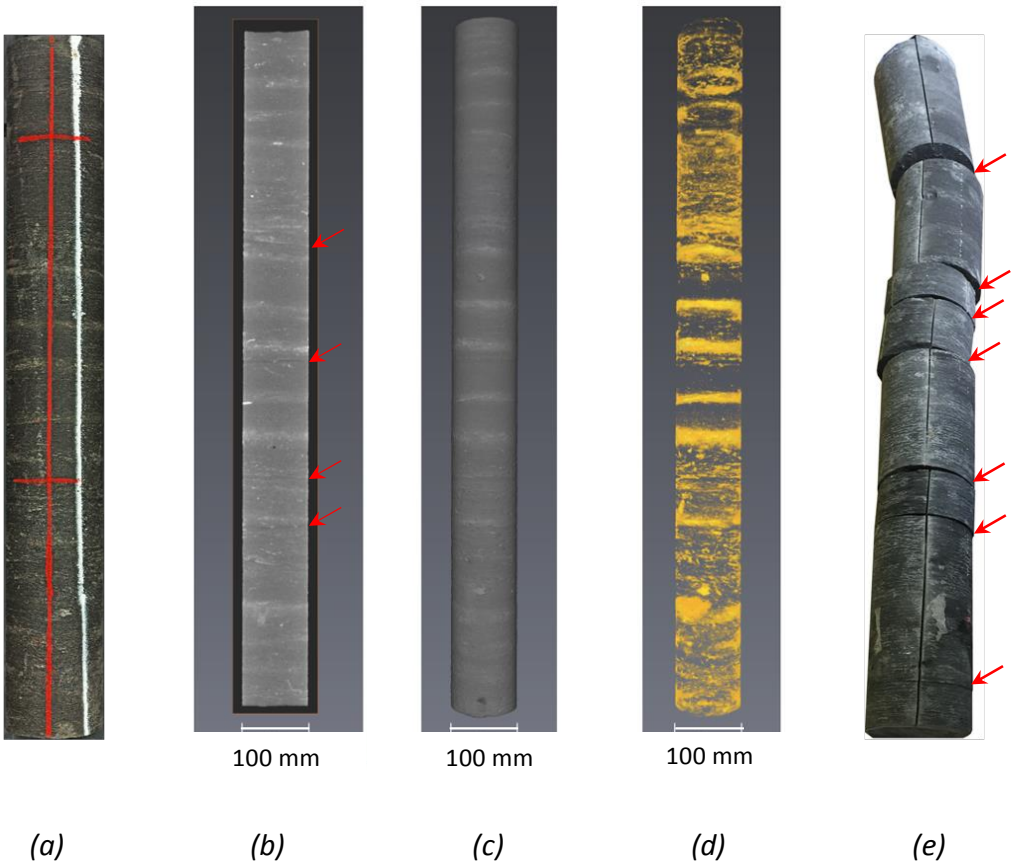

Figure 1. Photos and CT scans of core 5: a) Photo at initial state; b) to d) CT scan prior to sending to lab; e) Opening in lab.

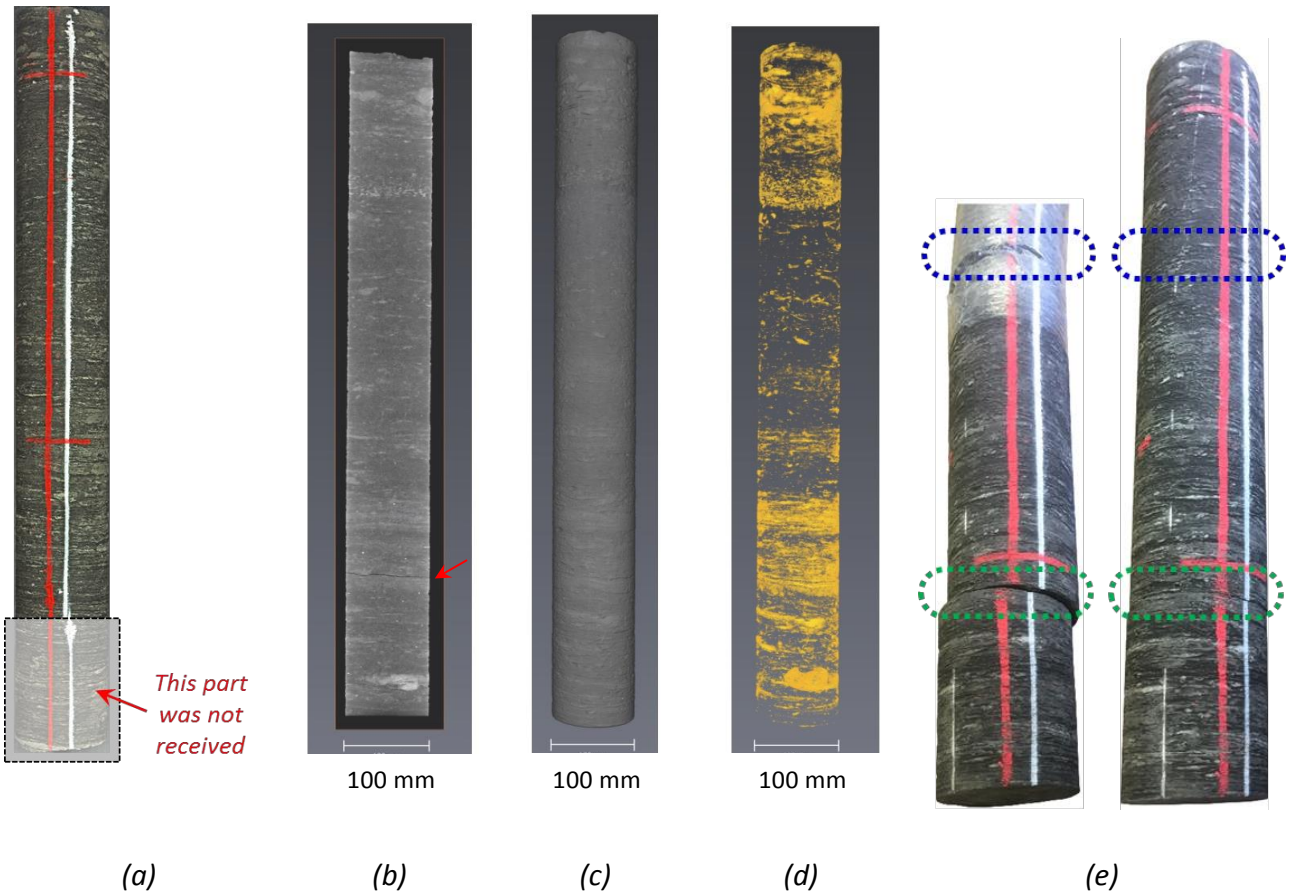

Figure 2. Photos and CT scans of core 7: a) Photo at initial state; b) to d) CT scan prior to sending to lab; e) Opening in lab.

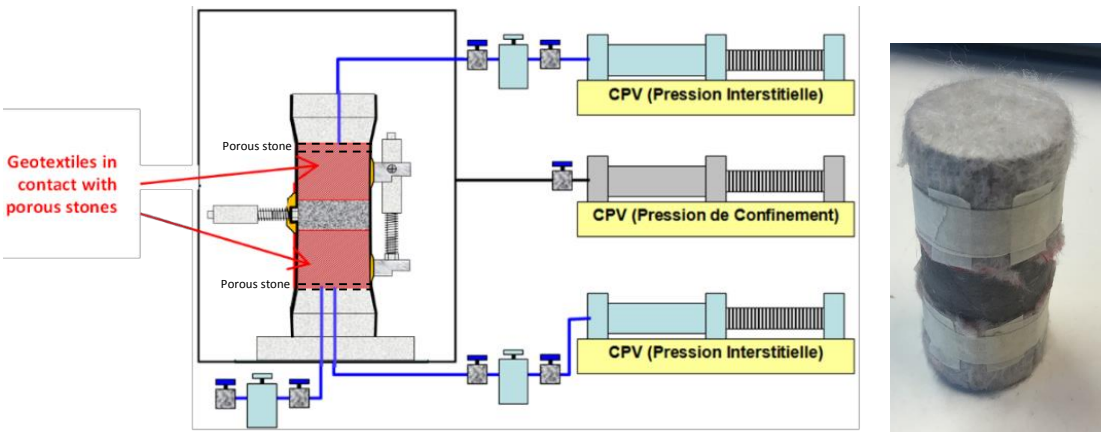

a *b*

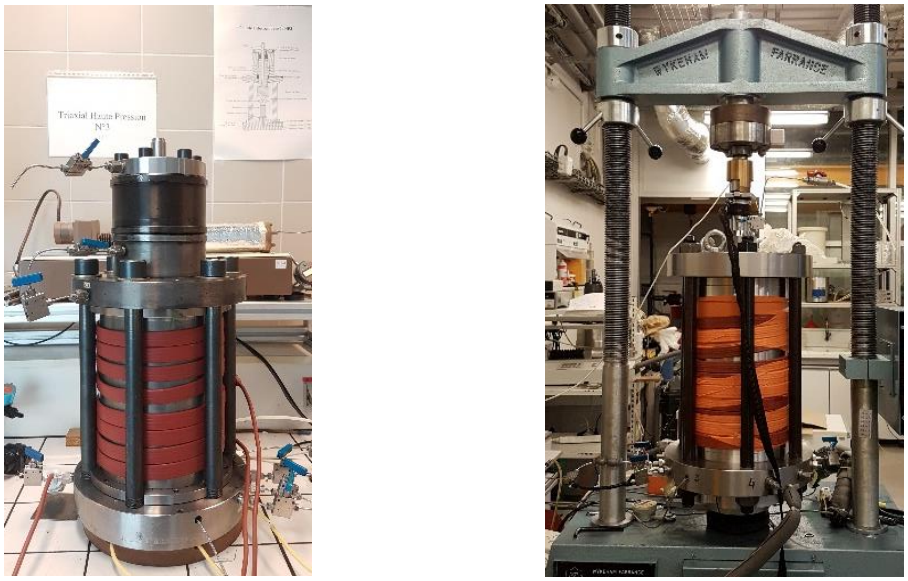

c *d*

Figure 3. a) Enhanced drainage system (with two geotextiles wrapped at top and specimen bottom and put in contact with porous disks) and connections with PVCs; b) Specimen wrapped into top and bottom geotextiles (see Belmokhtar et al. 2018 for more details); c) Autonomous self-compensated HP triaxial cell; d) Timo cell on a 25 tons triaxial press. Both cells are wrapped into an electric red ribbon aimed at controlling temperature at 25°C.

907

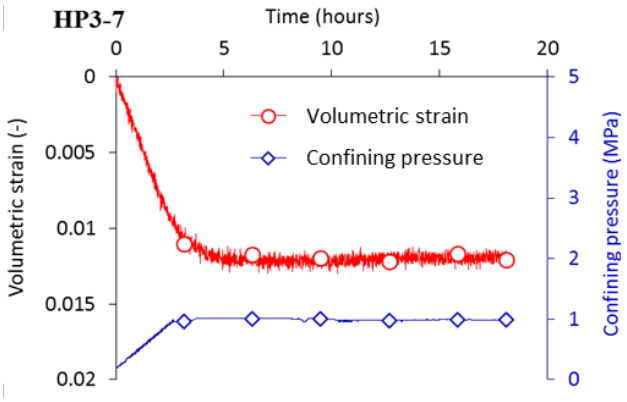

908

909 *Figure 4. Consolidation phase (σ' = 2.9 MPa, u_w = 1.9 MPa).*

910

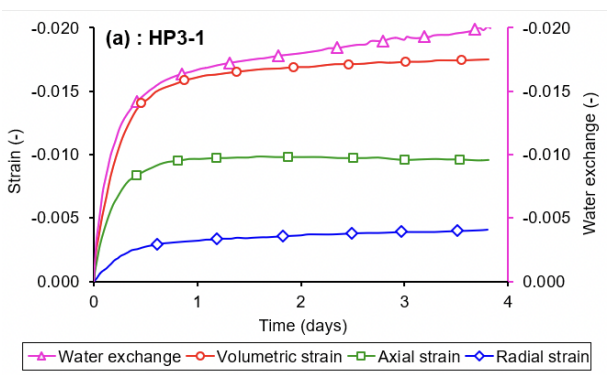

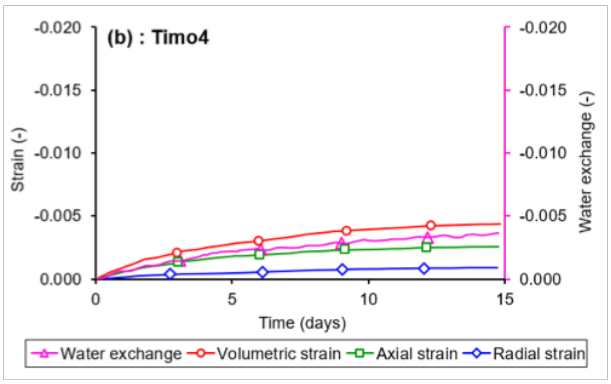

Figure 5. Saturation phase: a) *under 1 MPa (in-situ) effective stress (σ = 1.3 MPa, u_w = 0.3 MPa); b) under 5 MPa effective stress (σ = 6.9 MPa, u_w = 1.9 MPa)*

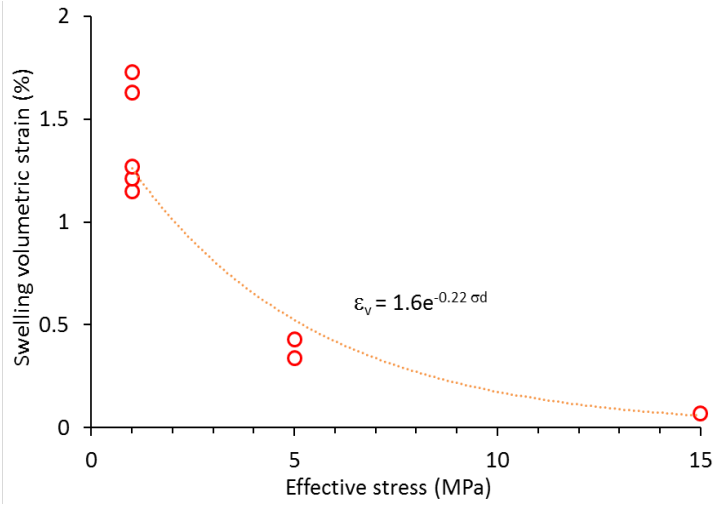

Figure 6. Monitored increases in volumetric strains under different effective confining stresses.

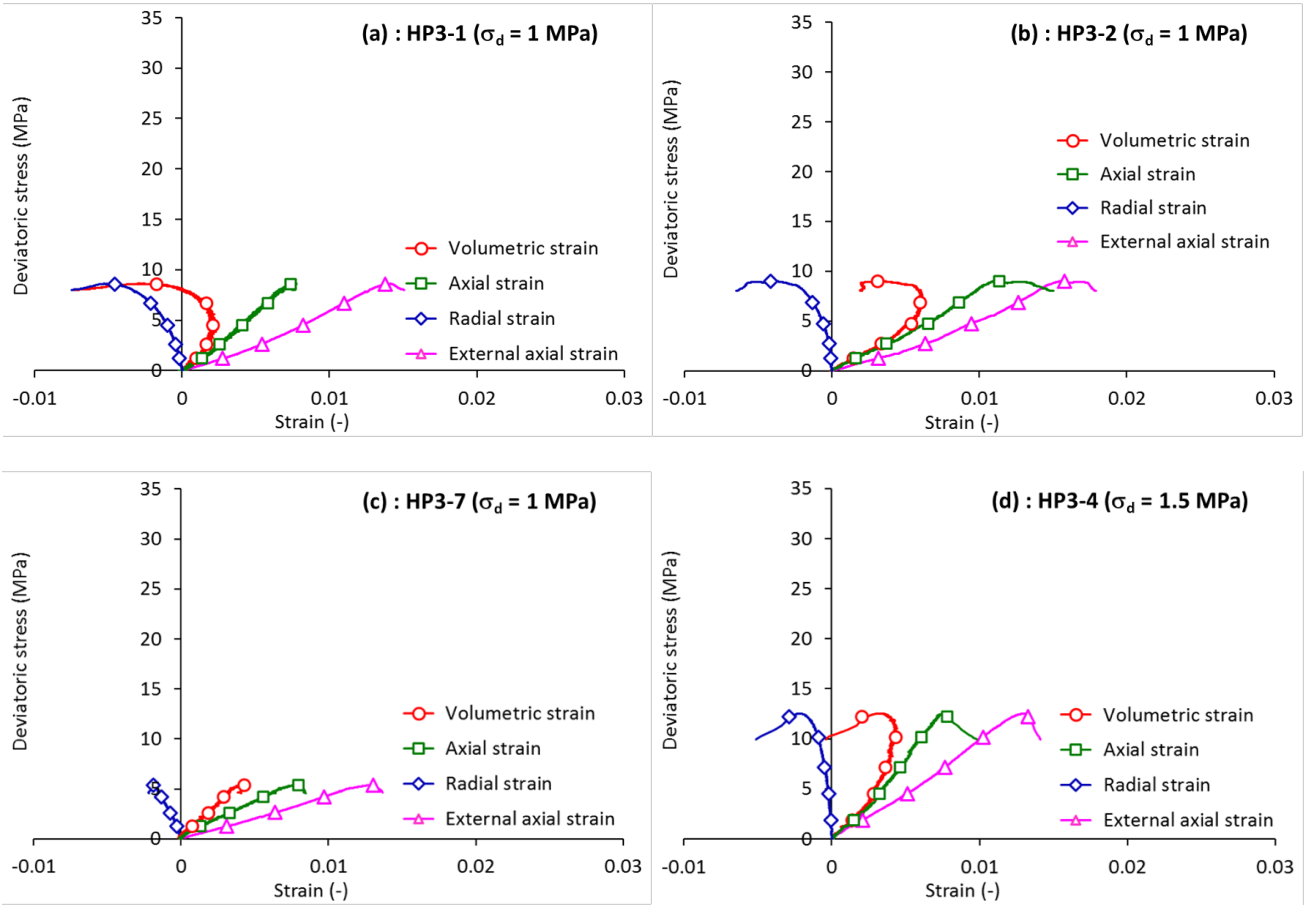

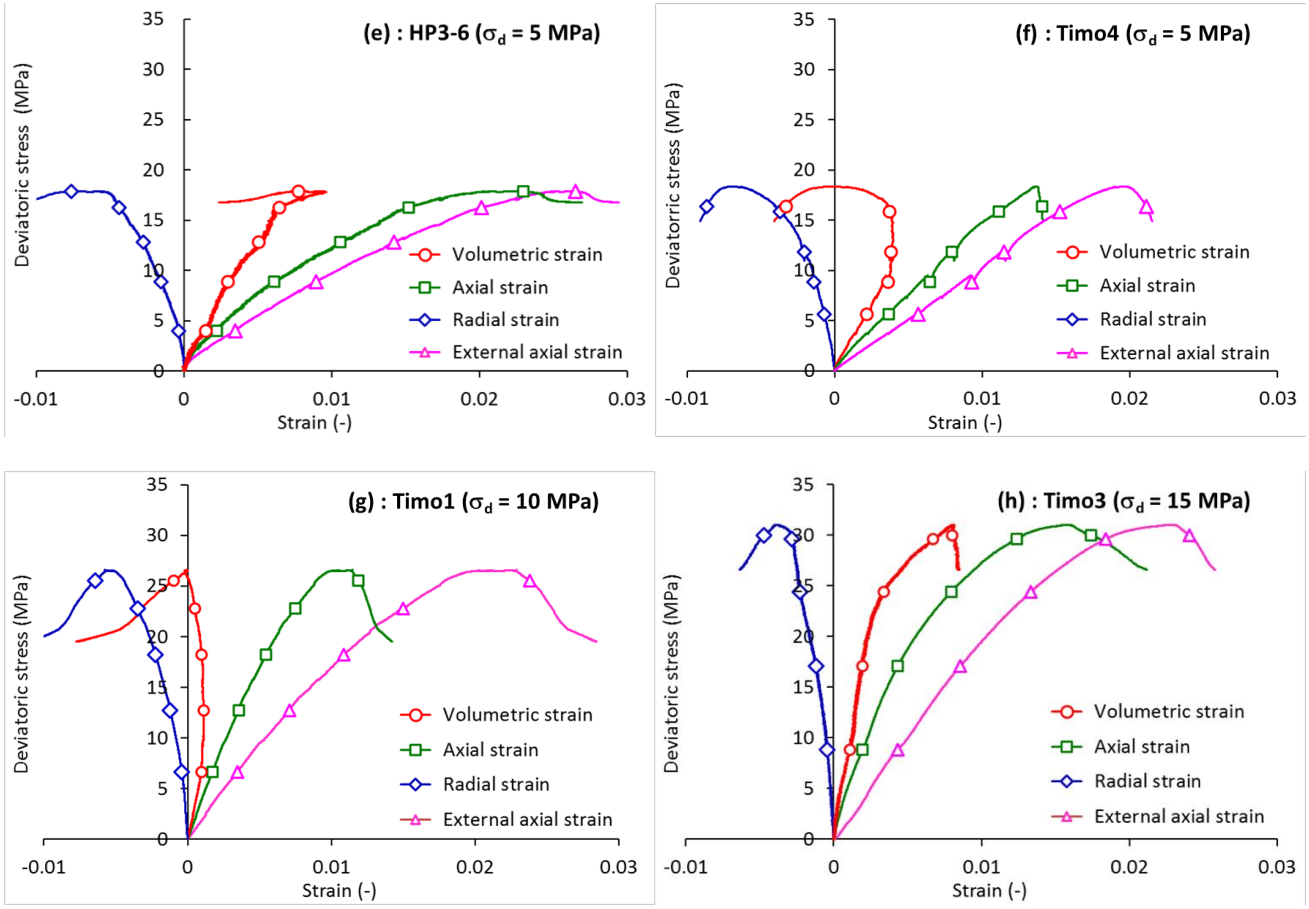

Figure 7. Drained triaxial shear tests.

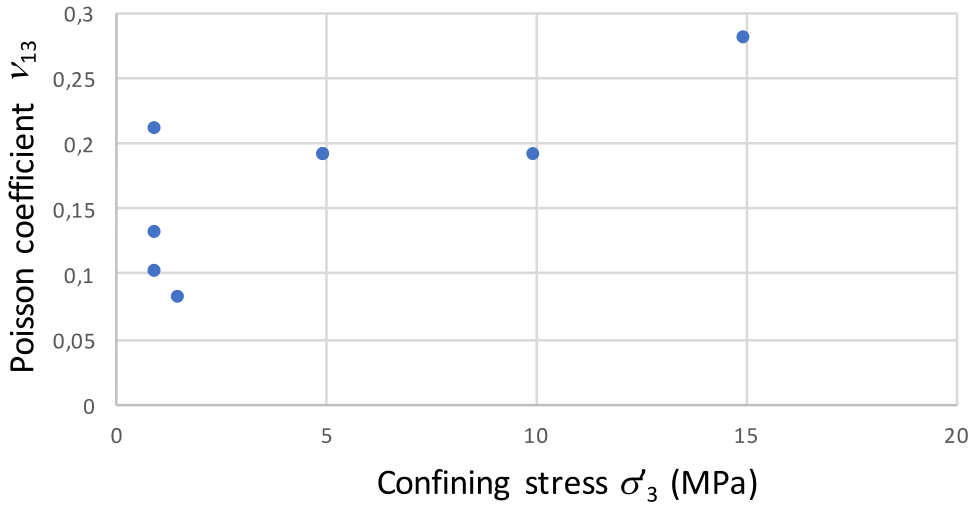

Figure 8. Changes in Poisson coefficient (from first loading) with respect to effective confining stress.

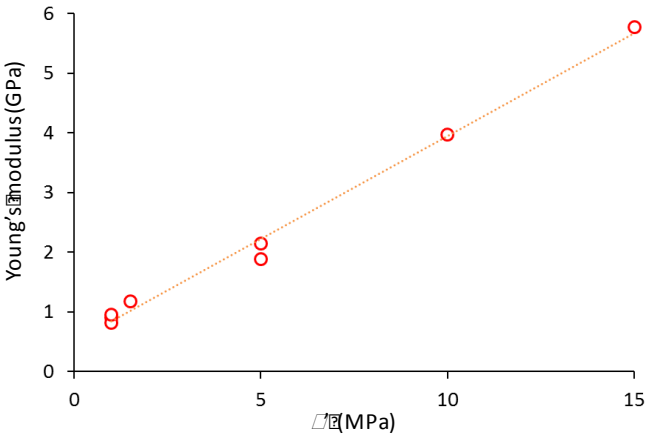

Figure 9. Changes in Young's modulus (from first loading) with respect to effective confining stress.

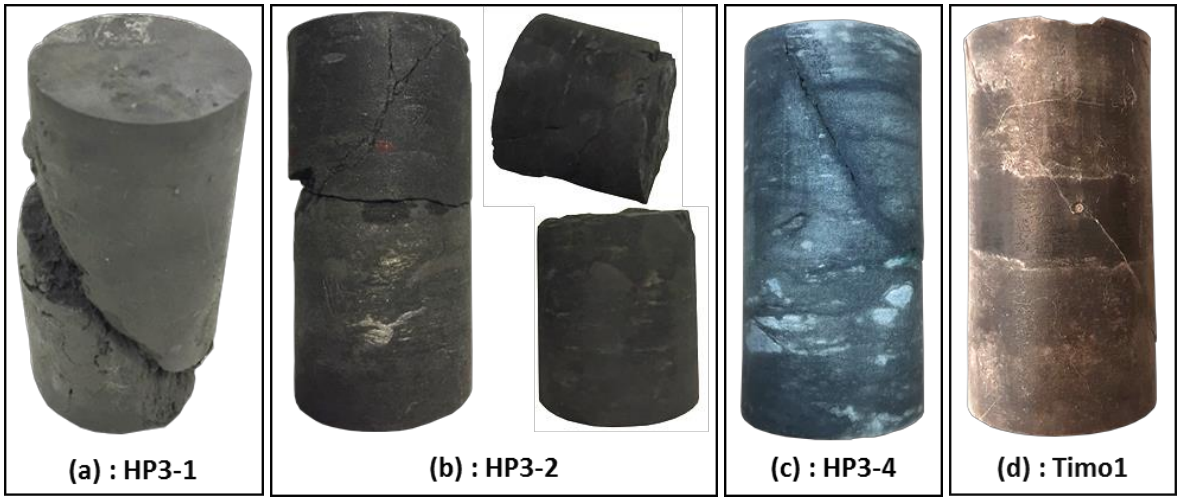

σ = 1.3 MPa	*σ = 1.3 MPa*	*σ = 1.3 MPa*	*σ = 11.9 MPa*
u = 0.3 MPa	*u = 0.3 MPa*	*u = 0.3 MPa*	*u = 1.9 MPa*

Figure 10. Photos of some sheared specimens.

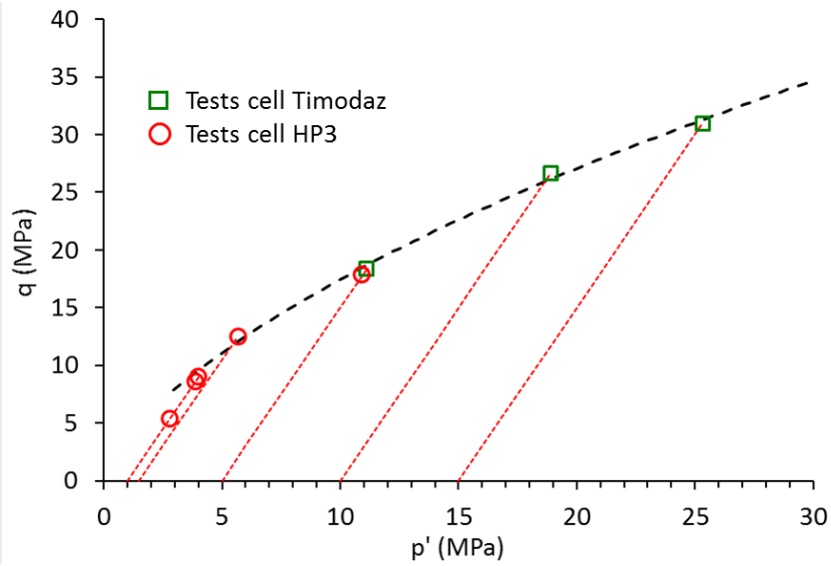

945

946 *Figure 11. Peak stresses obtained from drained tests with both devices*

947

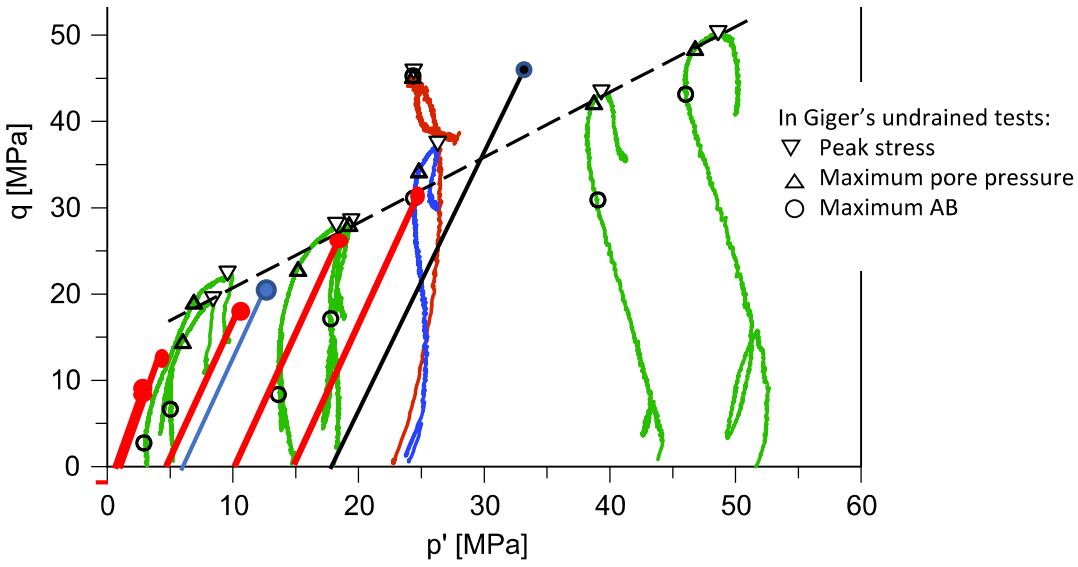

Figure 12. Comparison of the peak stresses from the present work (drained paths in thick red lines, strain rate of 6.6 x 10^{-8} s^{-1}) with the data of Giger et al. (2018) on specimens from same origin and depth (Lausen). Undrained shear paths at a rate of 2 x 10^{-7} s^{-1} are in green. Undrained tests at faster rates in dark red (2 x 10^{-5} s^{-1}) and blue (2 x 10^{-6} s^{-1}) provided larger peak stresses, see Chiu et al. 1986). The blue and black drained strain paths have been carried out by Giger et al. (2018) at a rate of 2 x 10^{-8} s^{-1}. In Giger's undrained tests, circles indicate the maximum AB values (A and B are the Skempton coefficients, Skempton 1954), upwards triangles correspond to the points at maximum pore pressure and downwards triangles represent the peak stresses.

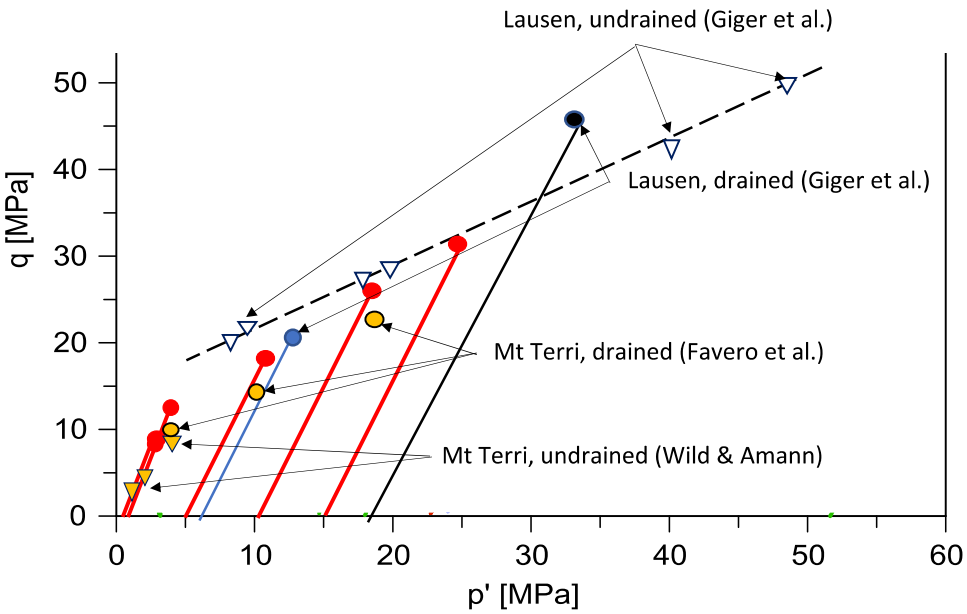

Figure 13. Comparison of peak stresses from drained and undrained tests on shallow Lausen specimens and deep Mt Terri ones. The drained tests data on Lausen specimens (ϕ = 12%) from this work (in red) are compared to the drained ones (in blue and black) of Giger et al. (2018) and also to the peaks from undrained tests (black dotted line). Data from Mt Terri specimens (ϕ = 17%) from drained tests (Favero et al. 2018) and undrained tests (Wild and Amman 2018a) are also represented.

978

979

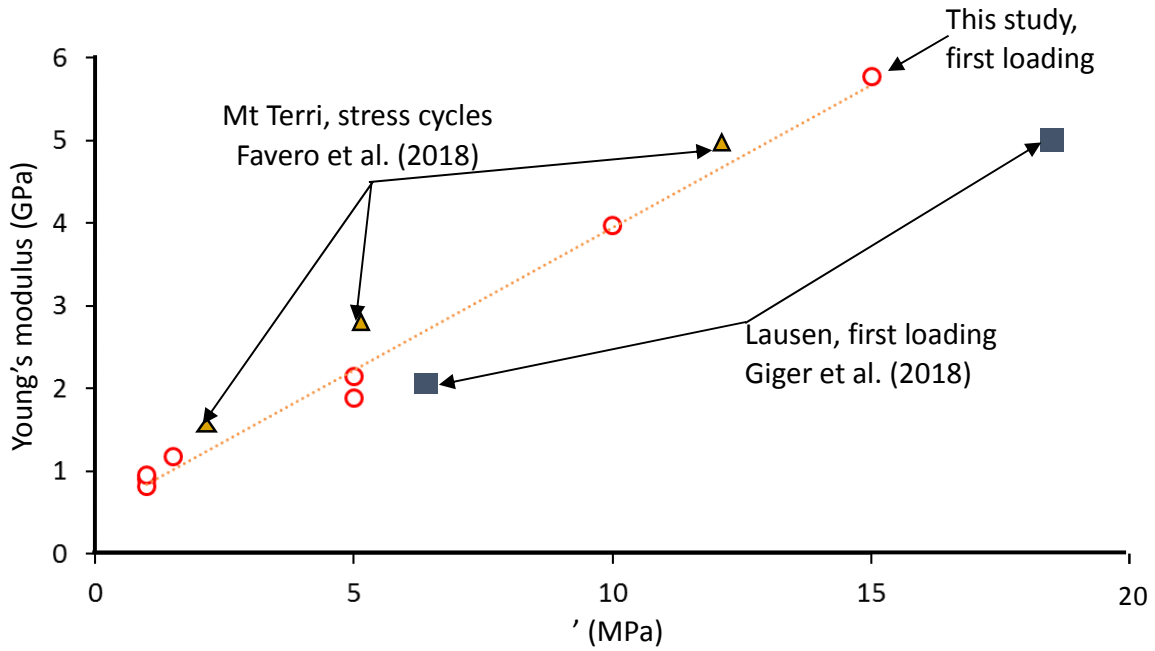

980

981 *Figure 14. Changes in Young modulus with effective confining stress: comparison with other available data on*
982 *Opalinus Clay (Favero et al. 2018, Giger et al. 2018).*

983

984

985

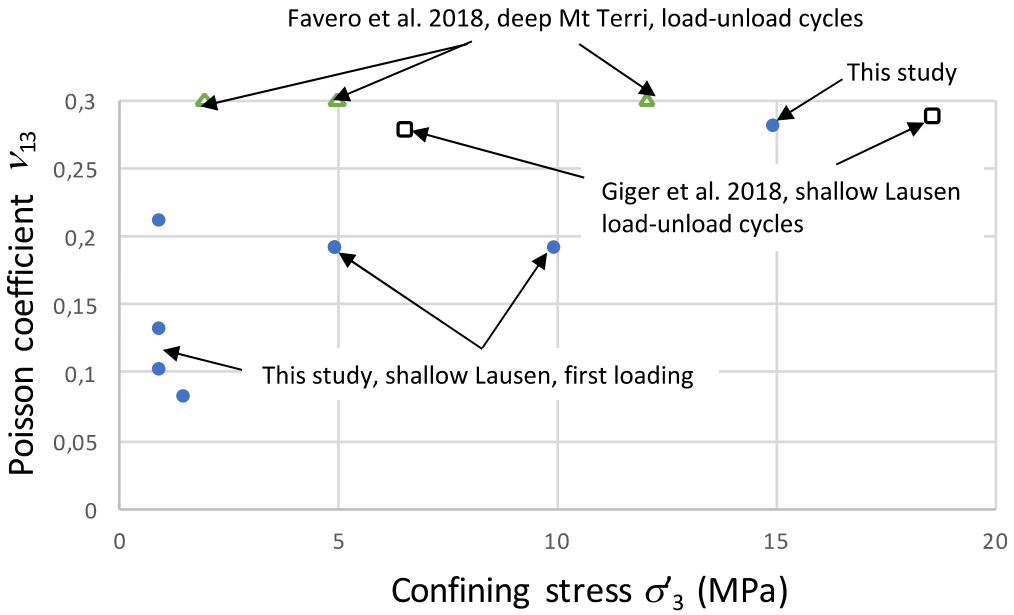

986

987 *Figure 15. Changes in Poisson coefficient ν_{13} with effective confining stress.*

988

989

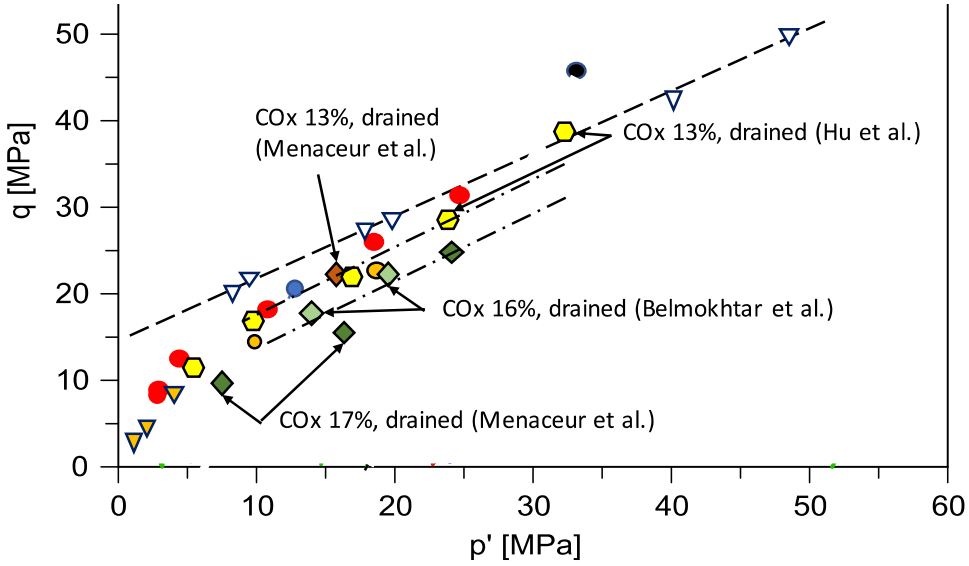

Figure 16. Comparison of the peak stresses of the Opalinus Clay (same data as in Figure 13) with that obtained on the Callovo-Oxfordian claystone through drained tests at various porosities by Hu et al. (2014), Menaceur et al. (2015) and Belmokhtar et al. (2018).

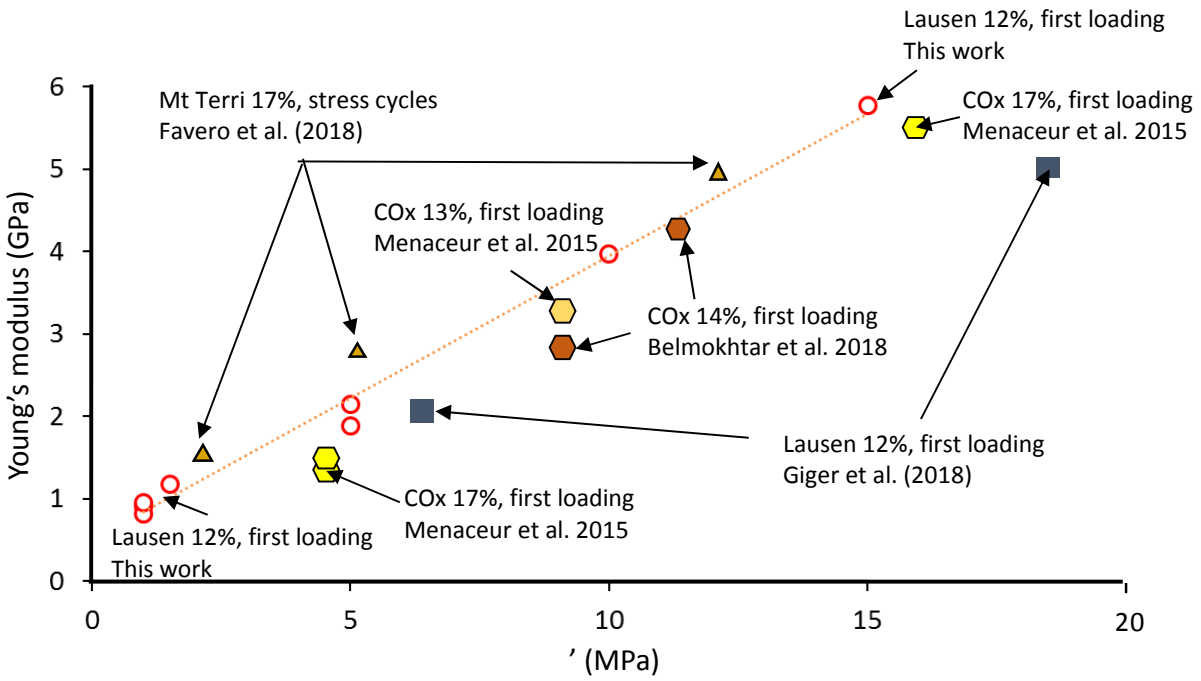

Figure 17. Comparison of the Young's moduli of the Opalinus Clay (same data as in Figure 14) with that obtained on the Callovo-Oxfordian claystone through drained tests at various porosities by Menaceur et al. (2015) and Belmokhtar et al. (2018).